Electronic Supplementary Material (ESI) for Journal of Materials Chemistry A.

Supporting Information

Tuning Photosensitization Efficiency of Atomically Precise Metal Nanoclusters by Super-Efficient and Exquisite Interface Modulation

Yu-Bing Li, Fang-Xing Xiao*

College of Materials Science and Engineering, Fuzhou University, Fuzhou, Fujian 350108, P.R. China.

Email: fxxiao@fzu.edu.cn

Table of Contents

Page NO.

Figure S1. The microscopic structure of NP-TNTAs……S6
Figure S2. TEM image and size distribution of Au_x@GSH and Pd@DMAP……S7
Scheme S1. Schematic illustration for construction of TNTAs@(Pd/Au_x)……S8
Figure S3. XRD, FTIR, and DRS of TNTAs@8A6P and TNTAs@6P8A ……S9
Figure S4. Transformed plots based on the Kubelka-Munk function vs. the energy of light……S10
Figure S5. Survey spectra, C 1s, Ti 2p and O 1s spectra of TNTAs and TNTAs@8A6P.……S11
Figure S6. XPS of TNTAs@6Pd……S12
Figure S7. FESEM images of TNTAs@6Pd, TNTAs@8Au_x and TNTAs@8A6P……S13
Figure S8. FESEM and EDS of TNTAs@6Pd……S14
Figure S9. STEM images of TNTAs@8A6P……S15
Figure S10. STEM image of TNTAs@6P8A with elemental mapping results……S16
Figure S11. FESEM and EDS of TNTAs@6Pd……S17
Figure S12. FESEM and EDS of TNTAs@8Au_x……S18
Figure S13. HER rates of pristine TNTAs, TNTAs@2Au_x, TNTAs@8Au_x and TNTAs@8A6……S19
Figure S14. HER performance of TNTAs, TNTAs@6Pd, TNTAs@8Au_x and TNTAs@8PxA……S20
Figure S15. Cyclic photocatalytic H_2 evolution of TNTAs@6P8A……S21
Figure S16. FTIR and XRD of TNTAs@8A6P……S22
Figure S17. XPS of TNTAs@8A6P after reaction……S23
Figure S18. C 1s spectra of TNTAs@8A6P……S24
Figure S19. TEM and HRTEM images of TNTAs@8A6P……S25
Figure S20. FTIR and XRD of TNTAs@6P8A……S26
Figure S21. PEC performance of TNTAs@8A6P and TNTAs@6P8A……S27
Figure S22. CV curves and energy level alignment of Au_x@GSH clusters……S28
Figure S23. PL of TNTAs@8A6P and TNTAs@6P8A……S29
Figure S24. Charge carrier densities (N_D) of TNTAs@8A6P and TNTAs@6P8A……S30
Figure S25. The energy level of TiO_2……S31
Table S1. Peak positions with corresponding functional groups……S32
Table S2. Chemical bond species *vs.* B.E.……S33
Table S3. A.Q.Y and S.T.H of TNTAs@8A6P.……S34
Table S4. A.Q.Y and S.T.H of TNTAs@6Pd……S35
Table S5. A.Q.Y and S.T.H of TNTAs@8Au_x……S36
Table S6. A.Q.Y and S.T.H of TNTAs@6P8A……S37
Table S7. Fitted EIS results……S38

References……S40

Experimental section

S1. Materials

Titanium sheets (50 mm × 20 mm × 0.1 mm, 99.9%), deionized water (DI H_2O, Millipore, 18.2 MΩ cm resistivity), graphite sheets (50 mm × 20 mm × 0.1 mm, 99.6%), ethylene glycol $(CH_2OH)_2$, ammonium fluoride (NH_4F), hydrogen fluoride (HF), nitric acid (HNO_3), sodium tetrachloropalladate (Na_2PdCl_4), tetraoctylammonium bromide (TOAB), toluene, sodium borohydride ($NaBH_4$), 4-dimethylaminopyridine (DMAP, $C_7H_{10}N_2$), sulfuric acid (H_2SO_4), sodium hydroxide (NaOH), *L*-glutathione (reduced, 98%, Sigma-Aldrich), gold (III) chloride trihydrate (99.9%, Sigma-Aldrich), Methanol (CH_3OH), Ethanol (C_2H_6O), Ethylene glycol ($C_2H_6O_2$), Glycerol ($C_3H_8O_3$), Lactic acid ($C_3H_6O_3$), Sodium sulfate (Na_2SO_4). All the materials are analytical grade and used as received without further purification.

S2. Fabrication of TNTAs

Preparation of TNTAs was referred to our previously published work.[S1] Ti foil was thoroughly cleaned by sonication in acetone, ethanol and DI H_2O. Then, Ti sheets were immersed in a mixed solution of HF–HNO_3–H_2O in a volume ratio of 1 : 4 : 5 for 30 s, washed by DI H_2O and dried with a N_2 stream. Anodization was carried out under ambient conditions at 50 V for 2 h with ca. 3 cm separation distance between the working (Ti foil) and counter electrode (graphite). The electrolyte consists of 0.3 wt % of NH_4F (0.6 g) in ethylene glycol (196 mL) and DI H_2O (4 mL). After anodization, TiO_2 nanotube arrays were washed by DI H_2O and dried with a N_2 stream. The surface layer was removed from Ti foil by sonication in ethanol for 5 min. A second anodization was performed at 50 V for 30 min to produce the TNTAs. Similarly, the resulting TNTAs were also washed by DI H_2O, dried with a N_2 stream and finally calcined at 450 ^oC for 3 h in air with a heating rate of 5 ^oC min^{-1}.

S3. Preparation of Au_x@GSH NCs

Preparation of Au_x@GSH NCs was referred to a previously published work.[S2] Preparation of Au_x@GSH clusters was referred to a previously published work. Briefly, gold (III) chloride trihydrate (40 mg) and L-glutathione (GSH, 46 mg) were thoroughly mixed in 50 mL of DI H_2O at ambient conditions. The mixture was continuously stirred until the appearance of a colorless solution and then was heated at 70 ℃ for 24 h. Subsequently, acetonitrile was added to the cluster solution to purify the clusters followed by washing several times with mixed solution of DI H_2O and acetonitrile (1:3 in volume). Finally, the clusters were re-dissolved in DI H_2O and stored at ambient conditions (0.8 mg/mL, pH = 3.98).

S4. Preparation of Pd@DMAP NYs

Preparation of Pd@DMAP NYs was referred to a previously published work.[S3] Preparation of Pd@DMAP nanoparticles was referred to a previously published method. Prior to the experiment, all glassware were cleaned thoroughly with aqua (3:1 in volume for HCl and HNO_3) for 12 h and thoroughly washed with DI H_2O. A 30 mM aqueous Na_2PdCl_4 solution (30 mL) was added to a 25 mM TOAB solution in toluene (80 mL). The transfer of the gold salt to the toluene phase can be seen

within a few seconds. A freshly prepared 0.4 M $NaBH_4$ (25 mL) aqueous solution was added to the above mixture under vigorous stirring, which causes an immediate color change from colorless to brown for Pd. After 30 min the two phases were separated and the toluene phase was subsequently washed with 0.1 M H_2SO_4, 0.1 M NaOH, and DI H_2O for three times, and then dried with anhydrous Na_2SO_4. Afterwards, an aqueous 0.1 M 4-dimethylaminopyridine (DMAP) solution (80 mL) was added to aliquots (80 mL) of the as-prepared nanoparticle mixtures. Direct phase transfer across the organic/aqueous interface was completed within 2 h with no stirring or agitation required. Finally, Pd-dissolved water phase was separated by a separatory funnel and Pd@DMAP aqueous solution (1.2 mg/mL) was thus obtained.

S5. Preparation of multilayered ternary and binary heterostructures

(a) Self-assembly of TNTAs@(Au_x/Pd) ternary heterostructures

TNTAs substrate was dipped into negatively charged Au_x@GSH NCs aqueous solution (0.8 mg/mL, 50 mL) for 10 s, washed with DI H_2O and dried with a gentle N_2 stream. Subsequently, Au_x-modified TNTAs was dipped into positively charged Pd@DMAP aqueous solution (0.06 mg/mL, 50 mL) for 10 s, after which the sample was subjected to the same washing and drying treatments, resulting in the TNTAs@(Au_x/Pd) ternary heterostructures. Concentration of Pd@DMAP NYs was controlled to be 0.03, 0.06, 0.12, 0.24 mg/mL via dilution by adding 1.25, 2.5, 5 and 10 mL of DI H_2O into pristine Pd@DMAP NYs aqueous solution, by which the corresponding samples were referred to as TNTAs@8A3P, TNTAs@8A6P, TNTAs@8A12P, and TNTAs@8A24P, respectively.

(b) Self-assembly of TNTAs@(Pd/Au_x) ternary heterostructures

Synthesis procedure of TNTAs@(Pd/Au_x) is analogous to TNTAs@(Au_x/Pd) apart from reversing the dipping sequence of TNTAs substrate in Au_x@GSH NCs and Pd@DMAP NYs (0.06 mg/mL, 50 mL) aqueous solutions. Concentration of Au_x@GSH NCs was controlled to be 0.1, 0.2, 0.4, 0.8 mg/mL by adding 6.25, 12.5, 25 and 50 mL of DI H_2O into pristine Au_x@GSH NCs aqueous solutions, by which the corresponding samples were referred to as TNTAs@6P1A, TNTAs@6P2A, TNTAs@6P4A and TNTAs@6P8A, respectively. The self-designed automatic machine based self-assembly apparatus was provided in the appendix section in SI.

(c) Self-assembly of TNTAs@Pd and TNTAs@Au_x binary heterostructures

TNTAs substrate was directly dipped into Pd@DMAP NYs aqueous solution (0.06 mg/mL, 50 mL) for 10 s, washed with DI H_2O and dried with a gentle N_2 stream, which gives rise to TNTAs@6Pd binary heterostructure. Analogously, TNTAs substrate was directly dipped into Au_x@GSH NCs aqueous solution (0.8 mg/mL, 50 mL) for 10 s and then subjected to the same washing and drying treatments, leading to the TNTAs@8Au_x binary heterostructure.

S6. Characterization

Zeta potentials were probed by dynamic light scattering analysis (ZetasizerNano ZS-90). Crystal structure was determined by X-ray diffraction (XRD, Miniflex600, Rigaku Corporation, Japan) using Cu Kα as the radiation source under 40 kV and 15 mA. Field-emission scanning electron microscopy (FESEM, Supra55, Carl Zeiss, Germany) was used to probe the morphologies of the samples. Transmission electron microscopy (TEM), high-resolution (HR) TEM and energy dispersive X-ray

spectrum (EDX) were collected on a Tecnai G2 F20 transmission electron microscope with an accelerating voltage of 200 kV. UV-vis diffuse reflectance spectra (DRS, Cary50, Varian, America) were obtained using $BaSO_4$ as the reflectance background ranging from 200 to 800 nm. Fourier transform infrared (FTIR) spectra were recorded on a TJ270-30A infrared spectrophotometer (Tianjin, China). X-ray photoelectron spectrometer (XPS) spectra were recorded on a photoelectron spectrometer (Escalab 250, Thermo Scientific, America), where binding energies (B.E.) of the elements were calibrated by 284.60 eV. Photoluminescence (PL) spectra were measured on a Varian Cary Eclipse spectrometer. Raman measurements were carried out on a Raman spectroscopy (Dxr-2xi, Thermo Scientific, America) with scan taken on an extended range from 0 to 3000 cm^{-1}. Energy levels of Au_x@GSH NCs were determined by Cyclic voltammetry (CV) measurements which were performed using a three-electrode system with glass carbon disk, platinum gauze, and Ag/AgCl (0.54 V vs. RHE) as the working, counter, and reference electrodes, respectively. The electrolyte was composed of 0.1 M tetraethylammonium perchlorate (TEAP) in acetonitrile (C_2H_3N) and purged with N_2 in a sealed vial for 10 min prior to use. CV curves were collected by sweeping at 0.1 V s^{-1} in a mixed C_2H_3N/TEAP (0.1 M) aqueous solution with adding 800 or 1000 μL of Au_x@GSH NCs.

S7. Photocatalytic hydrogen evolution measurements

Apparent quantum efficiency (Φ) and solar-to-hydrogen (S.T.H) of the reaction were determined according to our previously published work.[S[4-5]]

Apparent quantum efficiency (Φ) of the reaction was determined by the following equation:

$$\Phi(\%) = (2 \times \frac{R}{I}) \times 100$$

where R and I represent the number of evolved H_2 molecules and incident photons assuming all the incident photons are absorbed by the catalyst.

Solar-to-hydrogen (S.T.H) efficiency is calculated according to the following formula:

$$S.T.H = \frac{n_{H_2}\ (mmol) \times \Delta G(KJ/mol)}{S(cm^2) \times P(mW/cm^2) \times t(s)} \times 100\%$$

where, n_{H2} is the amount of H_2 molecules, ΔG is the Gibbs free energy per mol of H_2 (at 25 ℃, ΔG = 237 kJ mol^{-1}), S is the irradiation area, P is the light intensity, and t is the photoreaction time.

A.Q.Y and S.T.H efficiency were determined under the same experimental conditions except that a band pass interference filter centered at 360 ± 10 nm was equipped to provide photons with wavelengths between 355 and 365 nm. Filters of other bands (400, 420, 450, 500, 550, and 600 nm) were also used under the same conditions. In a typical calculation of A.Q.Y and S.T.H, the number of incident photons was measured using a radiant power energy meter (Perfect light, PLS-MW2000) with irradiation spot diameter of 2 cm. Cyclic photocatalytic H_2 evolution measurements were carried out as follows: photocatalytic reaction system was thoroughly degassed after the first run reaction without separating the photocatalysts or supplementing lactic acid and the thoroughly degassed reaction system was irradiated again under the same conditions.

S8. Photoelectrochemical (PEC) measurements

PEC measurements were carried out on an electrochemical workstation (CHI660E, CHI Shanghai, Inc.) with conventional three-electrode system and 0.5 M Na_2SO_4 aqueous solution (pH=6.69) was utilized as the electrolyte. The three-electrode system is composed of Pt foil (1 cm × 1 cm) which was used as the counter electrode and Ag/AgCl electrode as the reference electrode, and the working electrodes were prepared on fluorine-doped tin oxide (FTO) glass that was cleaned by sonication in DI H_2O and ethanol for 30 min and dried at 333 K in an oven. The boundary of FTO glass was protected using Scotch tape. Specifically, 10 mg of the sample was dispersed in 0.5 mL of ethanol by sonication to get slurry which was spread onto the pretreated FTO glass. After air drying, the Scotch tape was unstuck and the uncoated part of the electrode was isolated with nail polish.[S[6]] The exposed area of the working electrode was 1 cm^2. Finally, the working electrode was vertically dipped into the electrolyte and irradiated with visible light (λ>420 nm) (PLS-SXE300D, Beijing Perfect Light Co. Ltd., China). Potentials of the electrode were calibrated against the reversible hydrogen electrode (RHE) based on the following formula:

$$E_{RHE} = E_{Ag/AgCl} + 0.059pH + E^{o}_{Ag/AgCl} \ (E^{o}_{Ag/AgCl} = 0.1976 \text{ V at } 25 \text{ °C})$$

Transient photocurrent response (i.e., I-t) was collected under chopped light irradiation (light on/off cycle: 30 s) at a fixed bias of 1.23 V vs. RHE. Electrochemical impedance spectra (EIS) were measured on an electrochemical workstation (IM6, Zahner Germany) with an amplitude of 10 mV in the frequency ranging from 10^5 to 0.1 Hz.

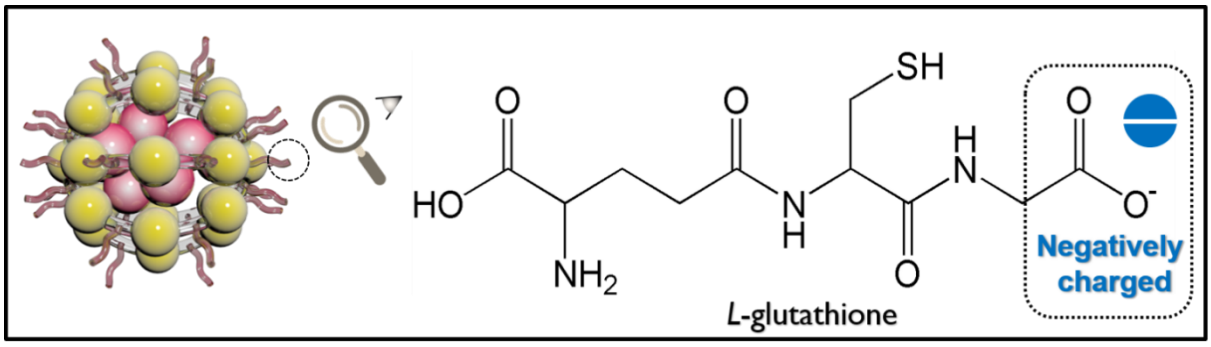

Note: GSH ligands capped on the Au_x@GSH NCs surface provide various polar functional groups including carboxyl (-COOH), amino (-NH_2), and amide (-CONH-) groups, among which deprotonated -COO^- specie endows Au_x@GSH NCs with a negatively charged surface that is beneficial for interaction with the positively charged TNTAs for electrostatic self-assembly buildup. Pd@DMAP NYs are featured by a positively charged surface, which enables electrostatic interaction with the negatively charged Au_x@GSH NCs. Alternatively, N-containing functional group in the DMAP ligand provides active sites to trigger the hydrogen bond interaction with the hydroxyl groups on the TNTAs surface. Apparently, surface ligands (DMAP & GSH) of Pd NYs and Au_x NCs play important roles in constructing TNTAs@Pd, TNTAs@Au_x, and TNTAs@(Au_x/Pd) heterostructures.[S[7]]

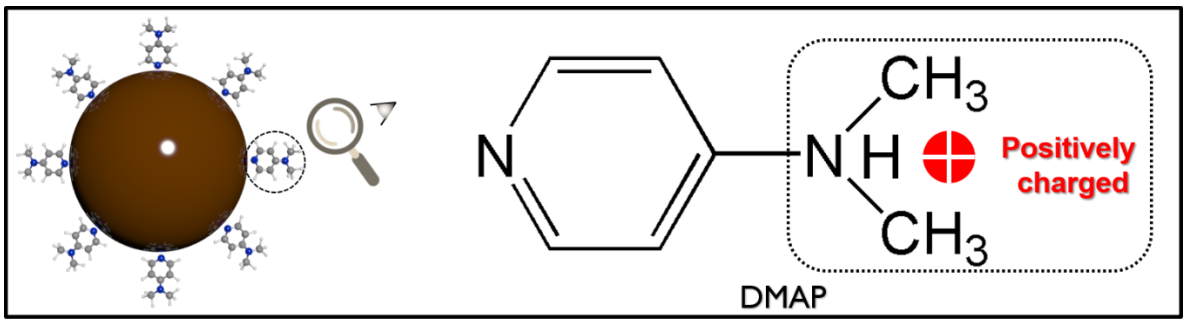

Note: Pd@DMAP NYs are characteristic of a positively charged surface over a wide pH (2-12) profile, which is reflected by the zeta potential results **(Fig. 1c**). DMAP ligands capped on Pd NYs form a labile donor-acceptor complex with the surface Pd atoms via the endocyclic nitrogen atoms, where surface charge arises from partial protonation of the exocyclic nitrogen atoms, giving rise to the positively charged surface.[S[8]] Atomically precise Au_x NCs are capped by a large amount of deprotonated carboxyl functional groups (-COO-) from the GSH ligands, which afford the negatively charged surface, as evidenced by the zeta potential results **(Fig. 1c)**. The Au_x@GSH NC is composed of a few gold-atom cores capped with thiolated shell (i.e., 1:1 ratio of Au : thiolate, having > 29 gold atoms).[S[9]]

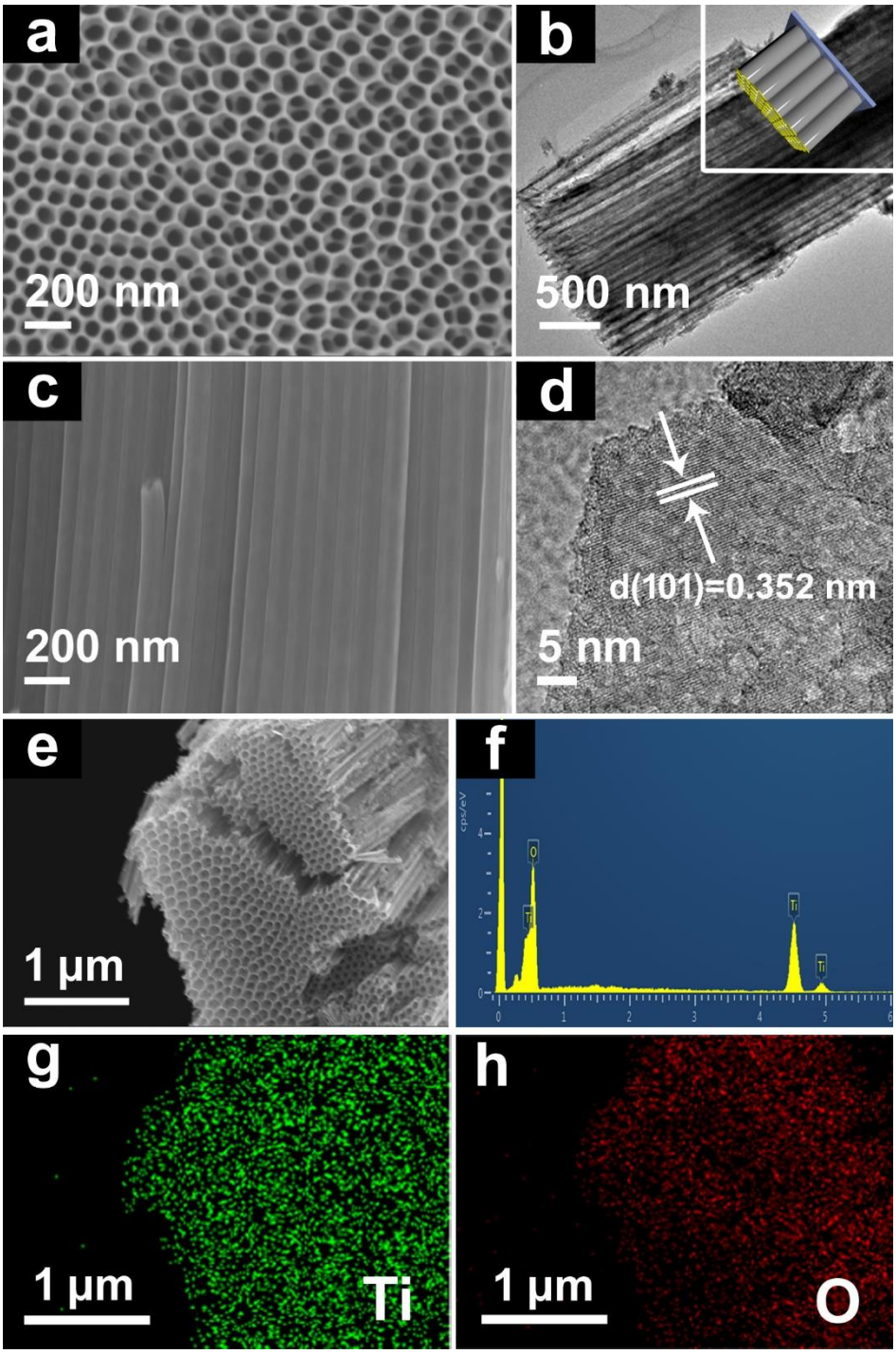

Fig. S1. (a) Top-view (c) cross-sectional FESEM images of TNTAs, (b) TEM, and (d) HRTEM images of TNTAs. (e) Low-magnified FESEM image of TNTAs with (f) EDS and (g & h) elemental mapping results.

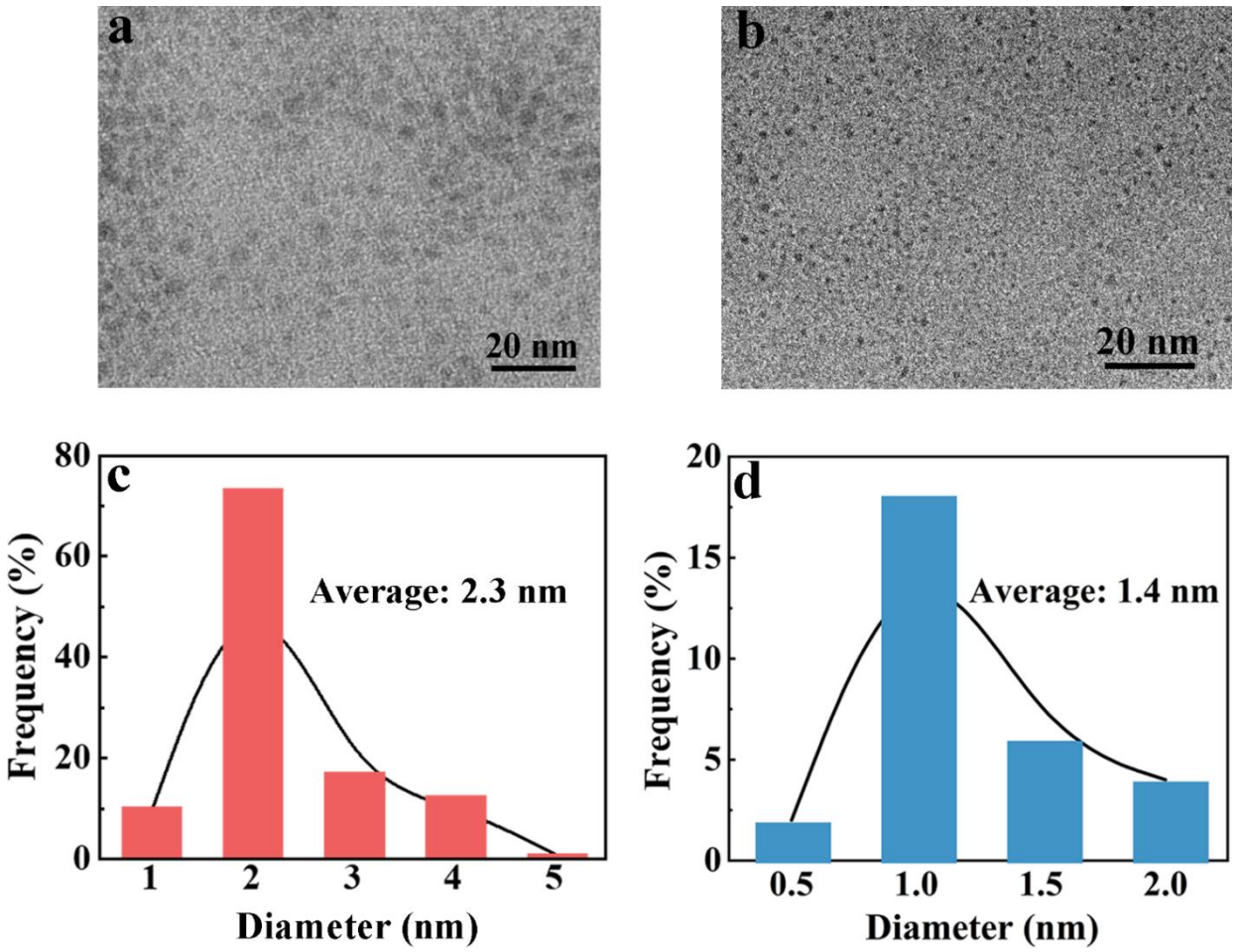

Fig. S2. TEM image and size distribution histograms of (a & c) Pd@DMAP NYs and (b & d) Au_x@GSH NCs.

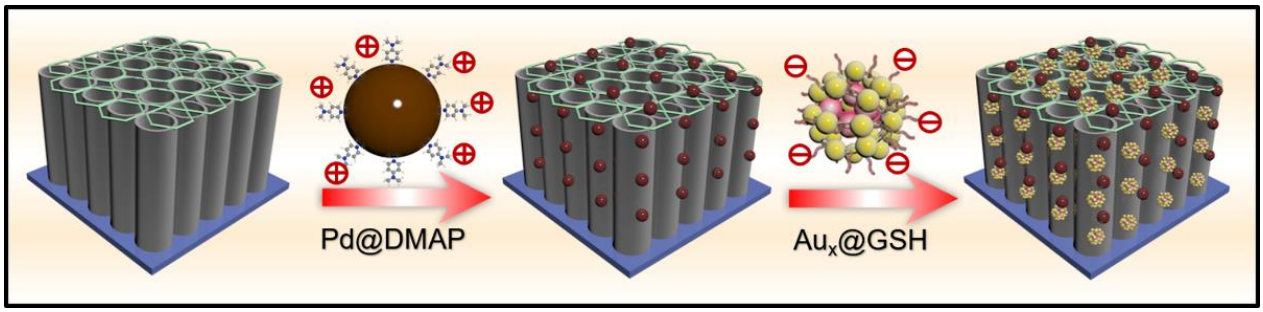

Scheme S1. Schematic illustration for self-assembly of TNTAs@(Pd/Au$_x$) ternary heterostructure.

Note: TNTA substrate is fabricated by a two-step electrochemical anodization method, and it serves as the substrate for fabricating TNTAs@(Pd/Au$_x$). Pd@DMAP NYs are then self-assembled on the TNTAs due to hydrogen bond interaction between DMAP ligands capped on the Pd NYs surface and hydroxyl (-OH) groups on the NP-TNTA surface. Finally, negatively charged Au$_x$@GSH NCs are electrostatically self-assembled with the positively charged TNTAs@Pd, resulting in the TNTAs@(Pd/Au$_x$) ternary heterostructure.

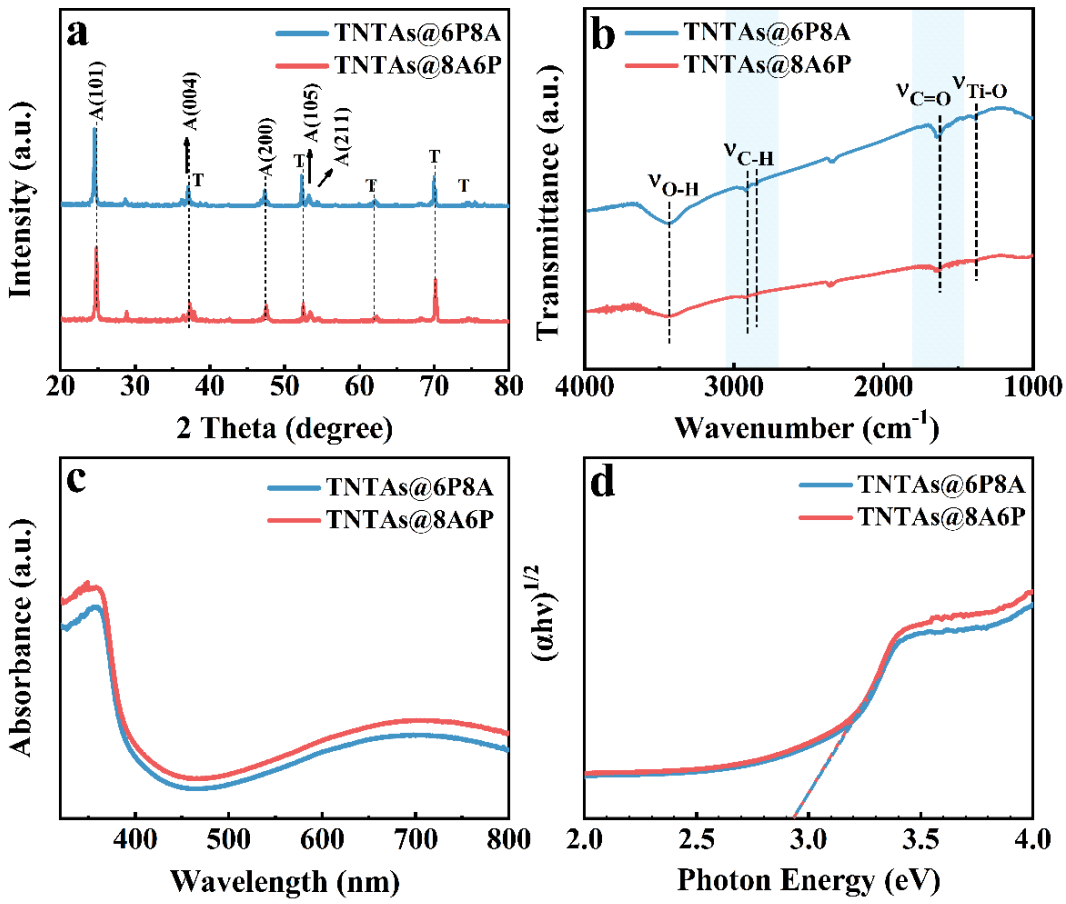

Fig. S3. (a) XRD patterns, (b) FTIR spectra, (c) DRS results, and (d) transformed plots based on the Kubelka-Munk function vs. the energy of light for TNTAs@6P8A and TNTAs@8A6P.

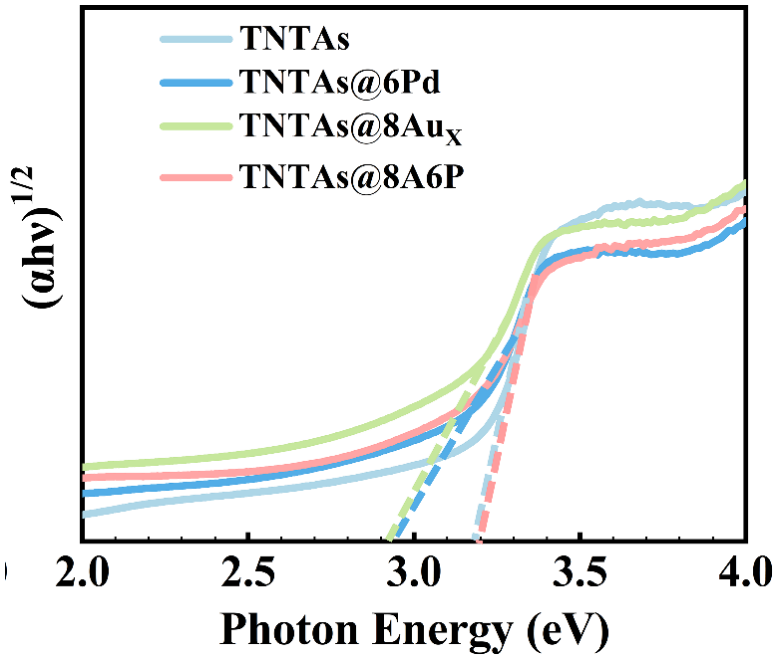

Fig. S4. Transformed plots based on the Kubelka-Munk function vs. the energy of light for TNTAs, TNTAs@6Pd, TNTAs@8Au$_x$, and TNTAs@8A6P.

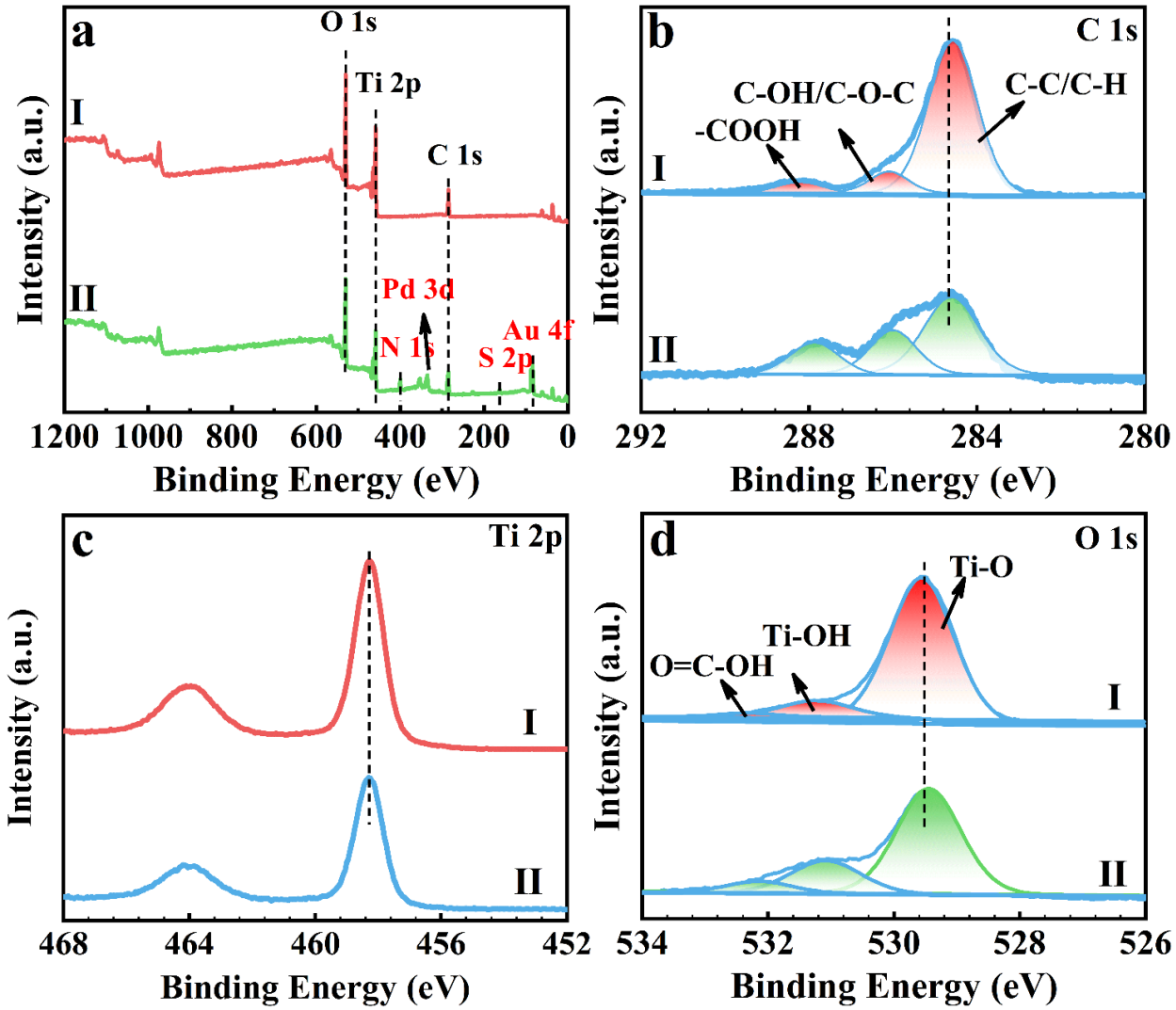

Fig. S5. (a) Survey spectra of TNTAs and TNTAs@8A6P; high-resolution (b) C 1s, (c) Ti 2p and (d) O 1s spectra of (I) TNTAs and (II) TNTAs@8A6P.

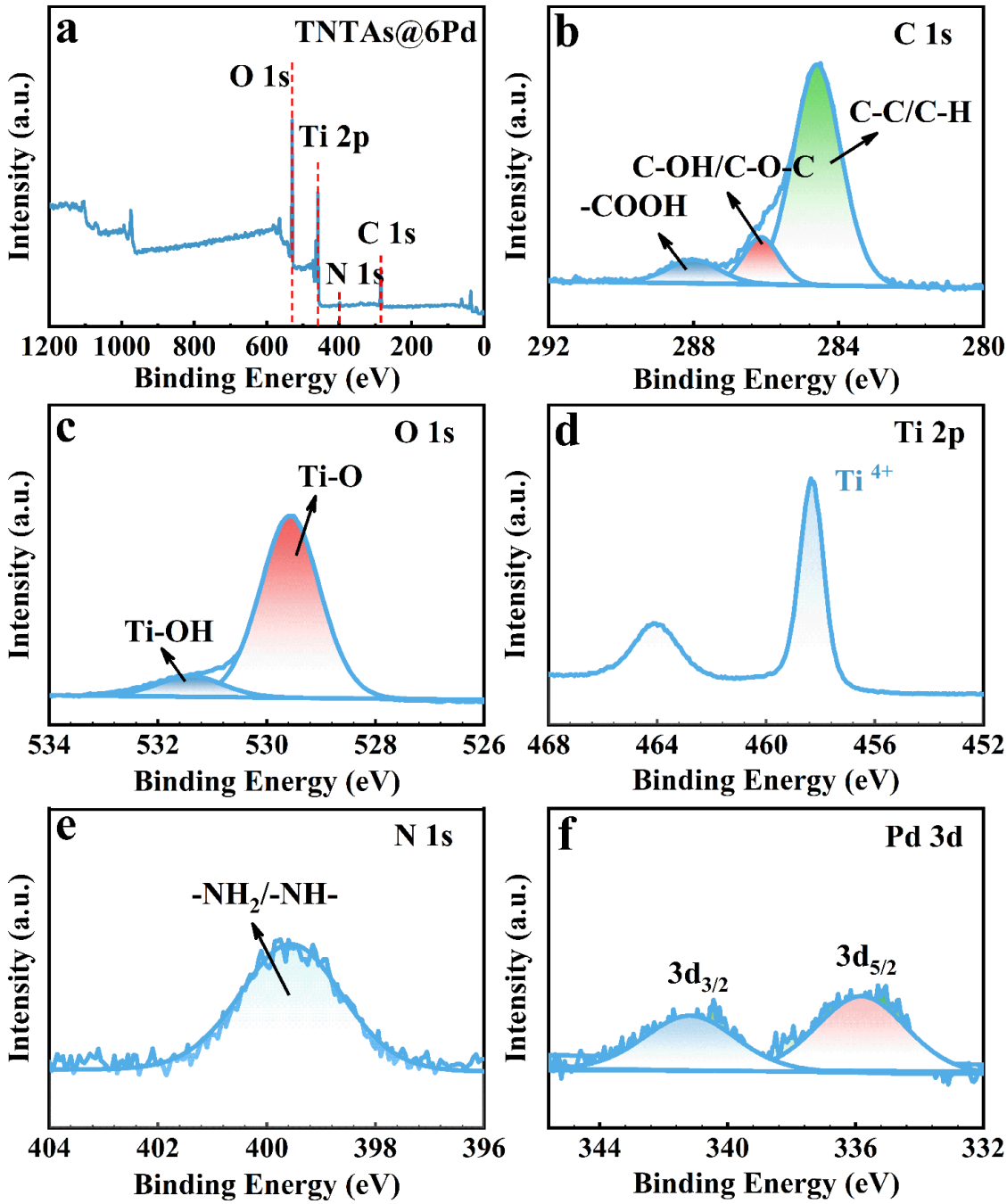

Fig. S6. (a) Survey and high-resolution (b) C 1s, (c) O 1s, (d) Ti 2p (e) N 1s, and (f) Pd 3d spectra of TNTAs@6Pd.

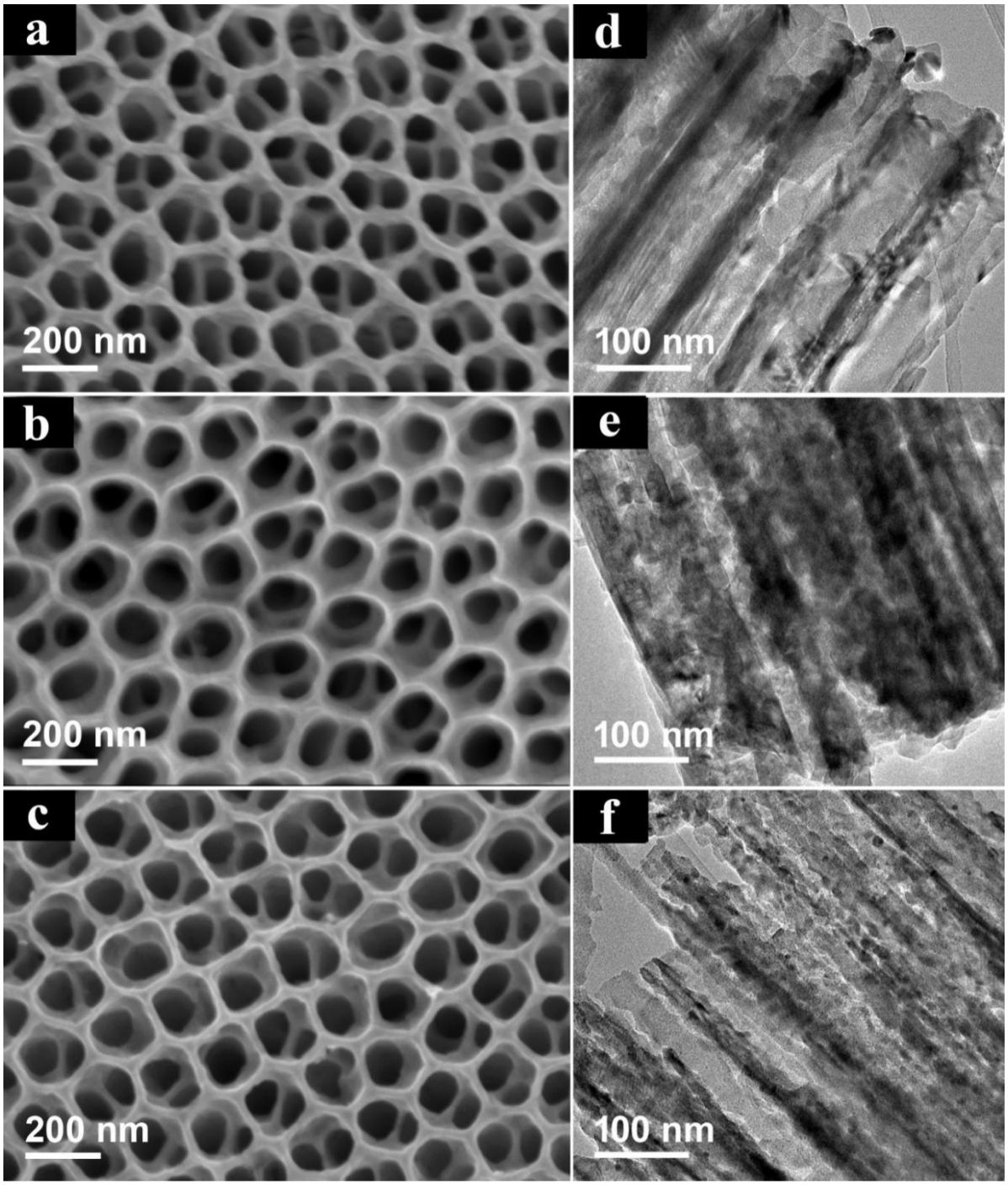

Fig. S7. Top-view FESEM and TEM images of (a &d) TNTAs@6Pd, (b & e) TNTAs@8Au$_x$ and (c & f) TNTAs@8A6P.

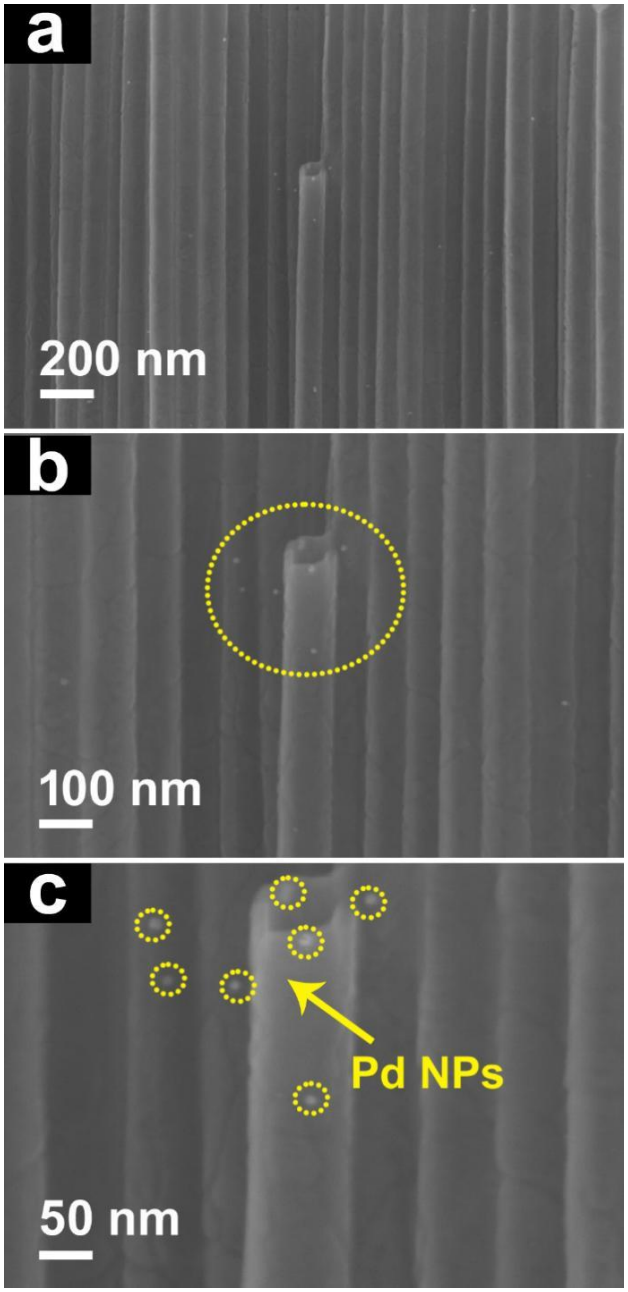

Fig. S8. (a-c) Cross-sectional FESEM images of TNTAs@6Pd.

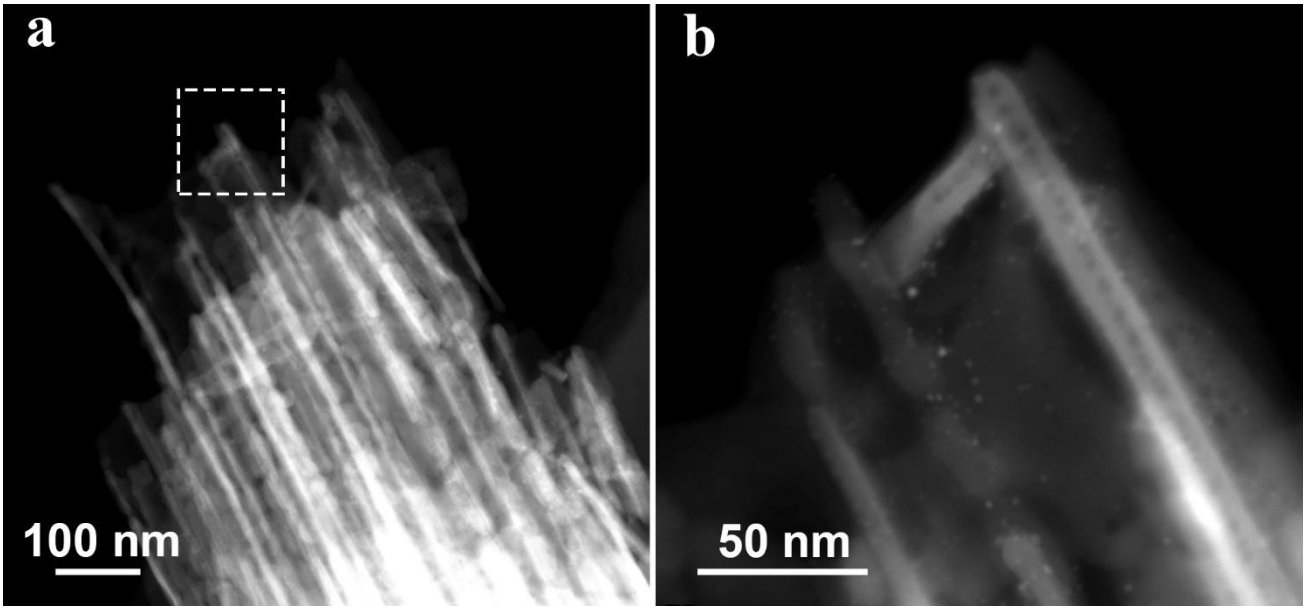

Fig. S9. STEM images of TNTAs@8A6P.

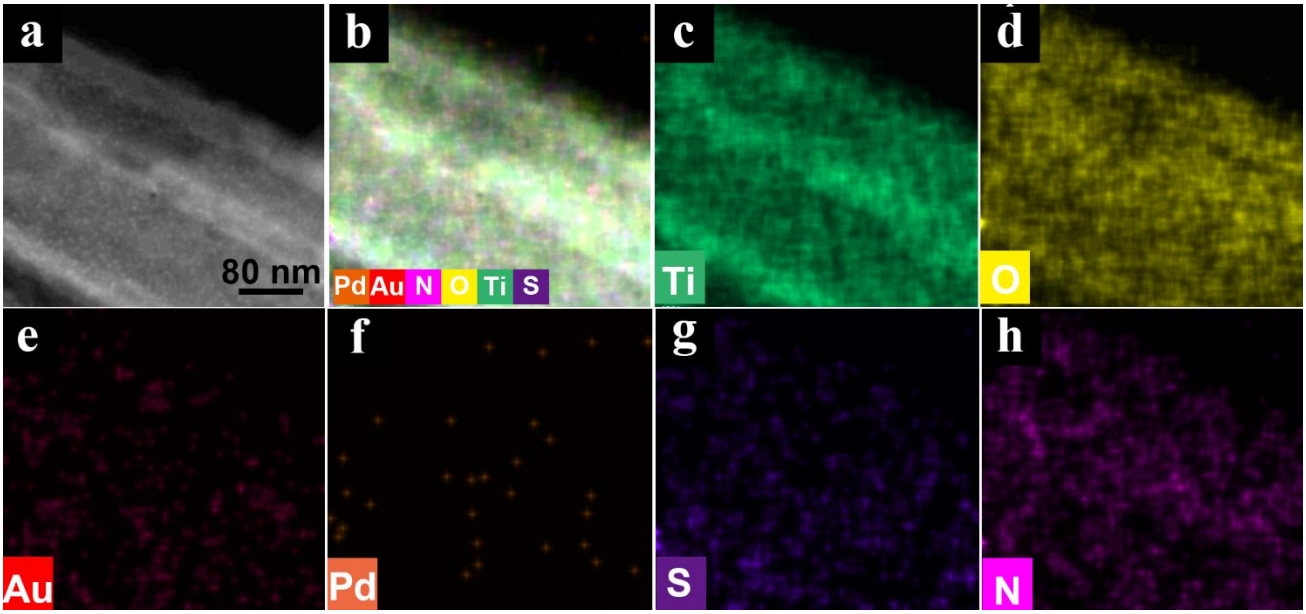

Fig. S10. (a) STEM image of TNTAs@6P8A with (b-h) elemental mapping results.

Note: The more enhanced Au signal relative to Pd is ascribed to the successive self-assembly of Pd@DMAP and Au_x@GSH NCs on the TNTAs substrate in TNTAs@6P8A. The S signal is from the GSH ligand of Au_x NCs and N signal arises from the DMAP ligand of Pd NYs.

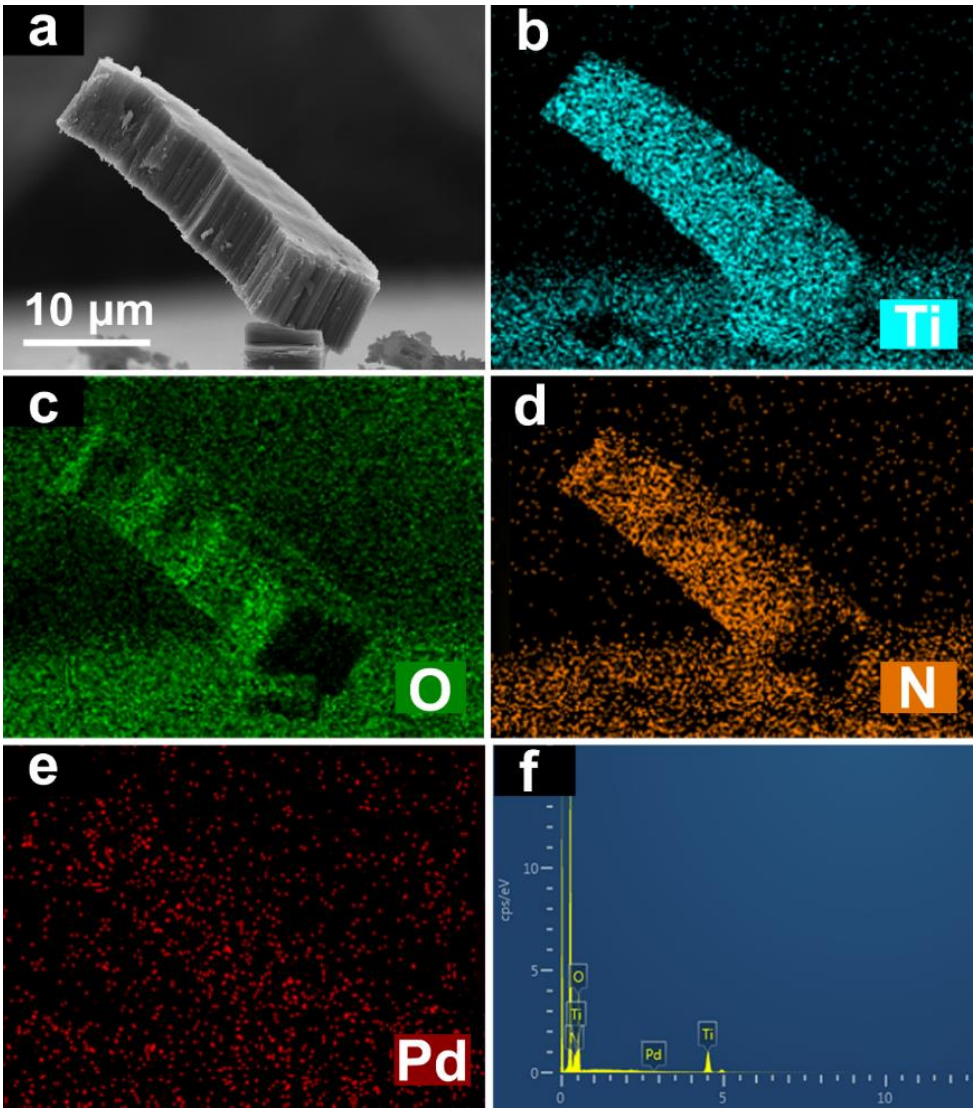

Fig. S11. (a) FESEM image of TNTAs@6Pd with (b-e) elemental mapping and (f) EDS results.

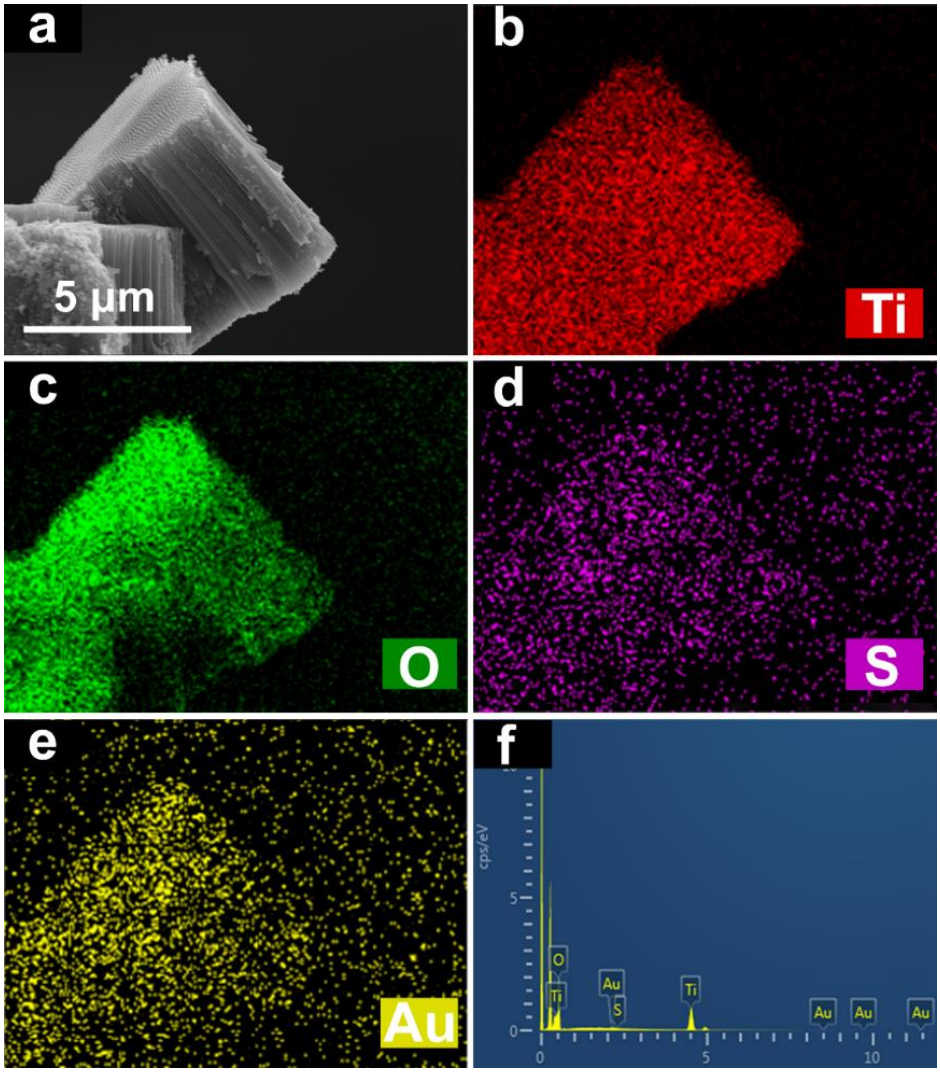

Fig. S12. (a) FESEM image of TNTAs@8Au$_x$ with (b-e) elemental mapping and (f) EDS results.

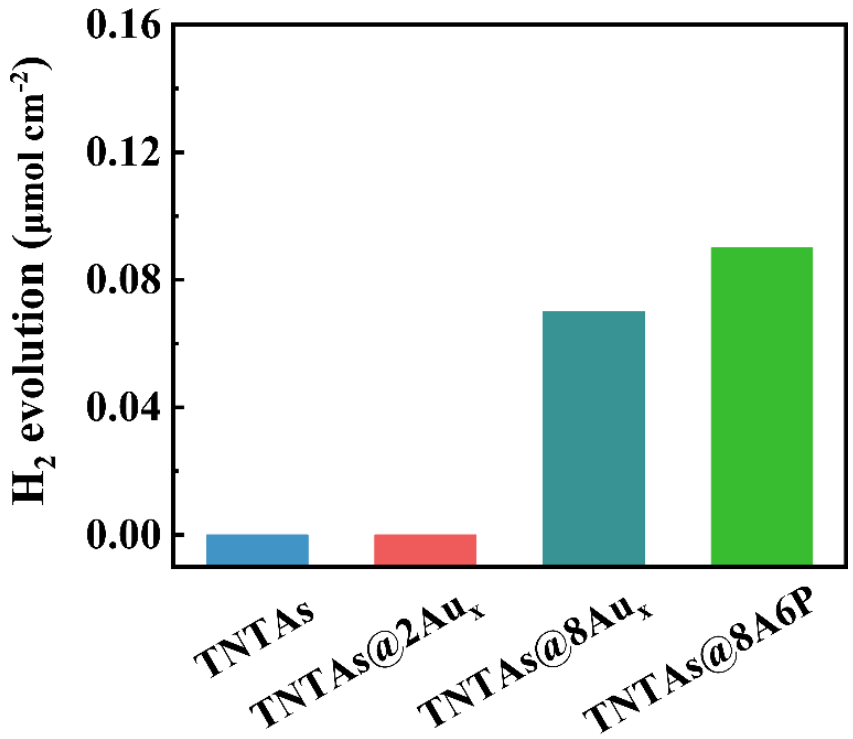

Fig. S13. Photocatalytic H_2 evolution rates of TNTAs, TNTAs@2Au$_x$, TNTAs@8Au$_x$, and TNTAs@8A6P under visible light irradiation (λ>420 nm) for 2 h.

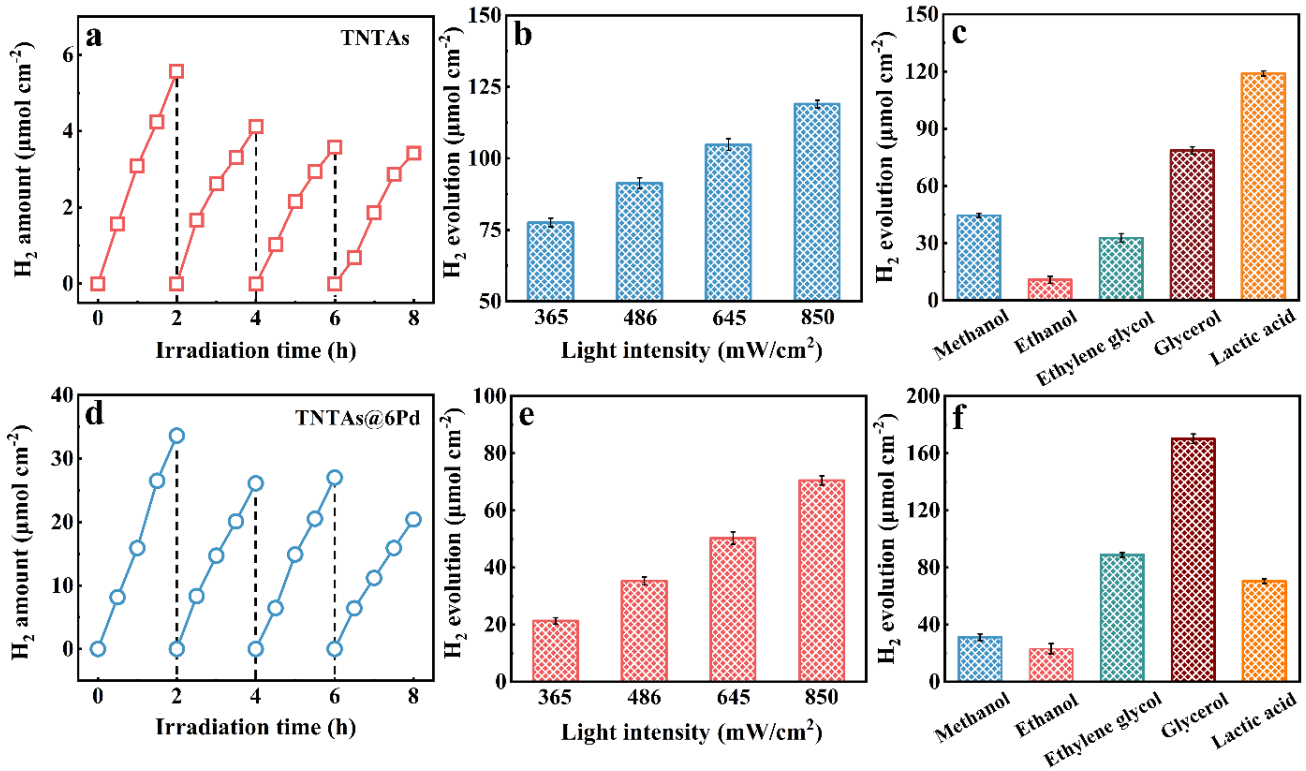

Fig. S14. Cyclic photocatalytic H_2 evolution performances of (a) TNTAs and (d) TNTAs@6Pd under continuous simulated solar light (200 nm<λ<800 nm) irradiation for 8 h, photocatalytic H_2 evolution rates of (b) TNTAs@8A6P and (e) TNTAs@6P8A under simulated solar light irradiation with different light intensity (365, 486, 645, 850 mW/cm^2) and photocatalytic H_2 evolution performances of (c) TNTAs@8A6P and (f) TNTAs@6P8A in the presence of different sacrificial reagents under simulated solar light (200 nm<λ<800 nm) irradiation.

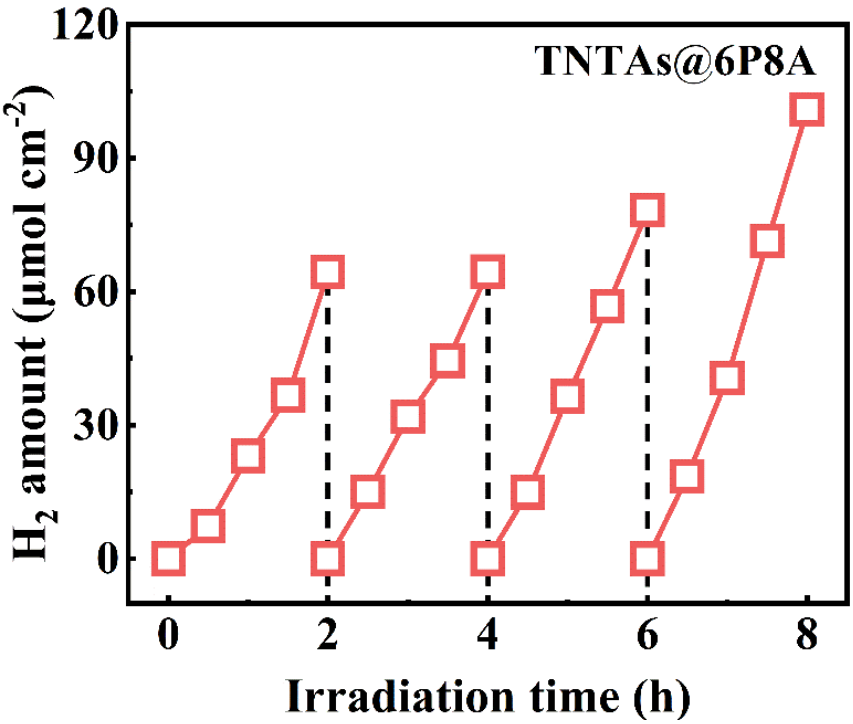

Fig. S15. TNTAs@6P8A under continuous simulated solar light (200 nm<λ<800 nm) irradiation for 8 h.

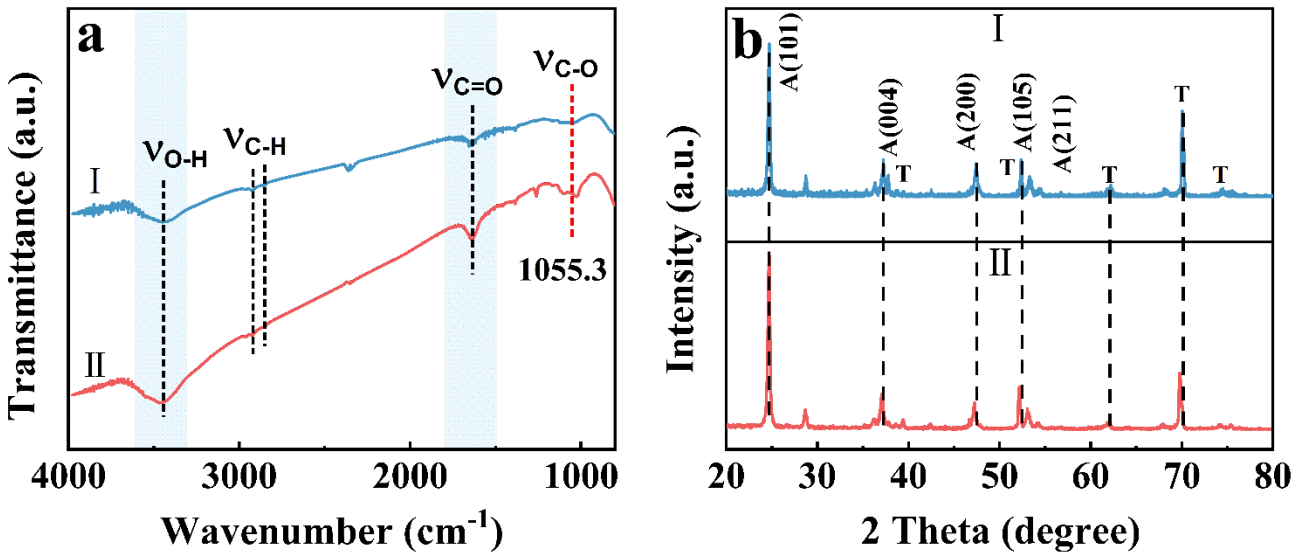

Fig. S16. (a) FTIR spectra and (b) XRD patterns of TNTAs@8A6P (I) before and (II) after cyclic reactions.

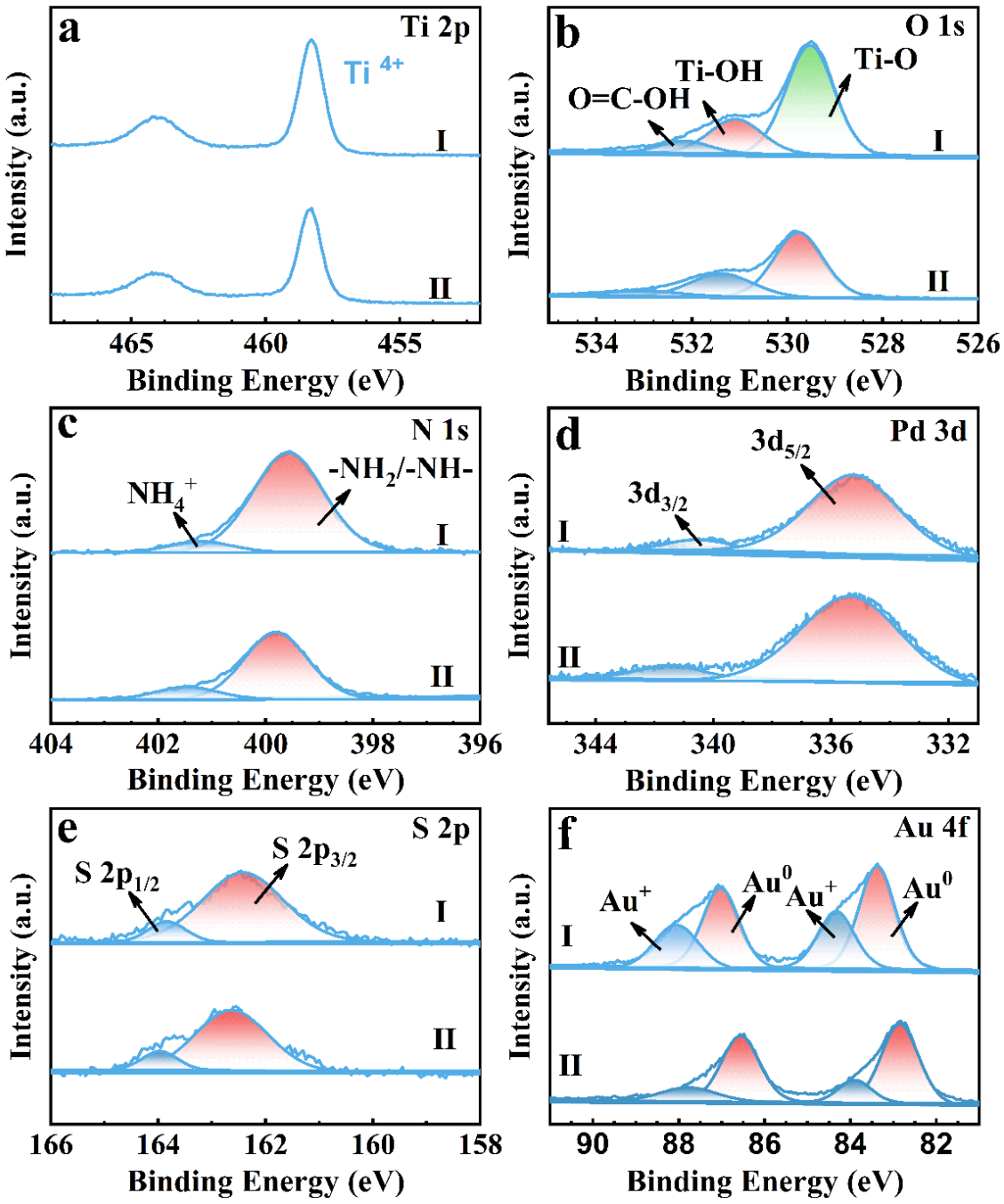

Fig. S17. High-resolution (c) Ti 2p, (d) O 1s, (e) N 1s, (f) Pd 3d, (g) S 2p and (h) Au 4f spectra of TNTAs@8A6P (I) before and (II) after cyclic reactions.

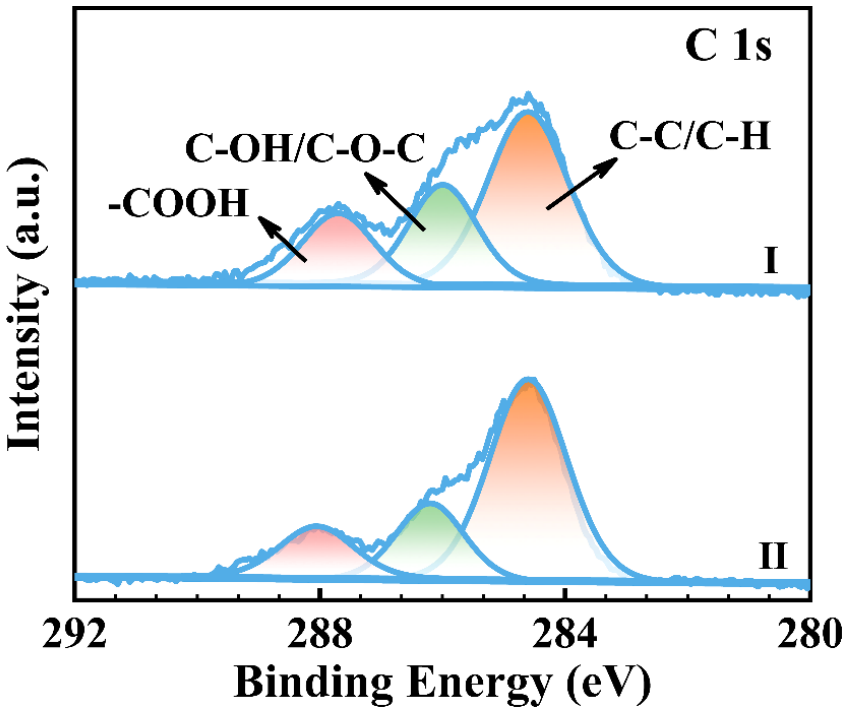

Fig. S18. High-resolution C 1s spectra of TNTAs@8A6P (I) before and (II) after cyclic reactions.

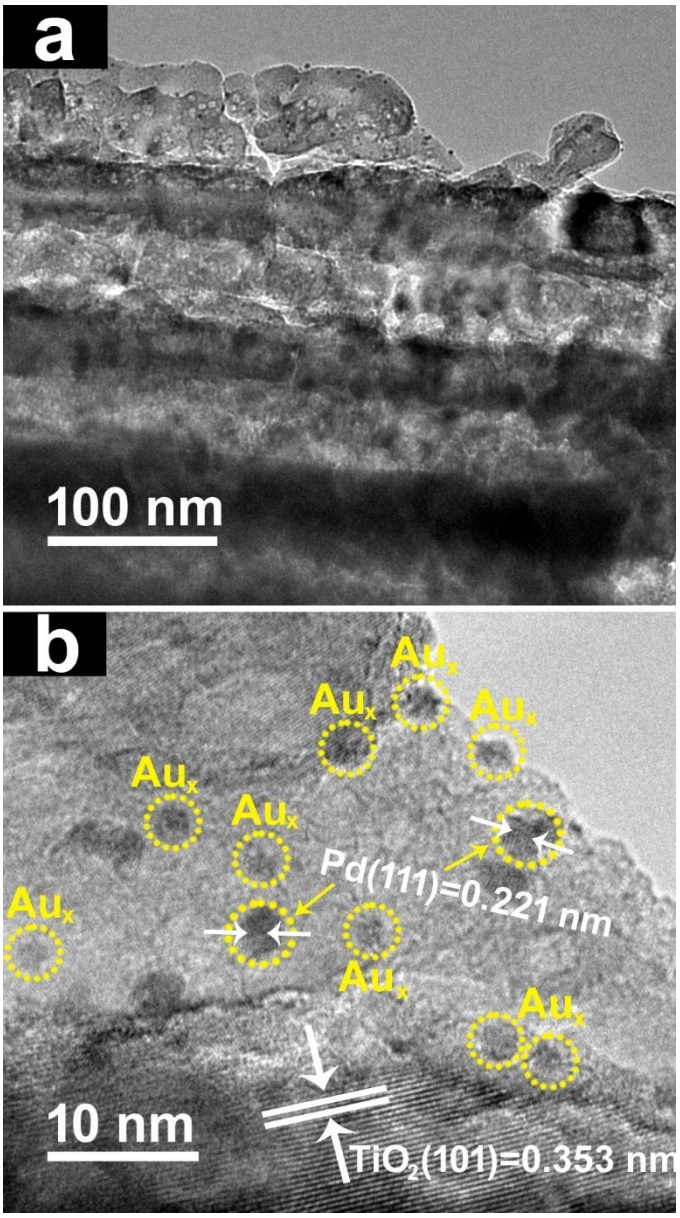

Fig. S19. (a) TEM and (b) HRTEM images of TNTAs@8A6P after cyclic reactions.

Note: A large amount of amorphous Au_x@GSH NCs are found in the HRTEM image of TNTAs@8A6P after cyclic reactions, indicating atomically precise Au_x@GSH NCs are retained even after continuous simulated solar light irradiation, which might be ascribed to the protection of Pd@DMAP NYs on the outermost layer, which retards the *in-situ* self-transformation of Au_x@GSH NCs to Au NPs.

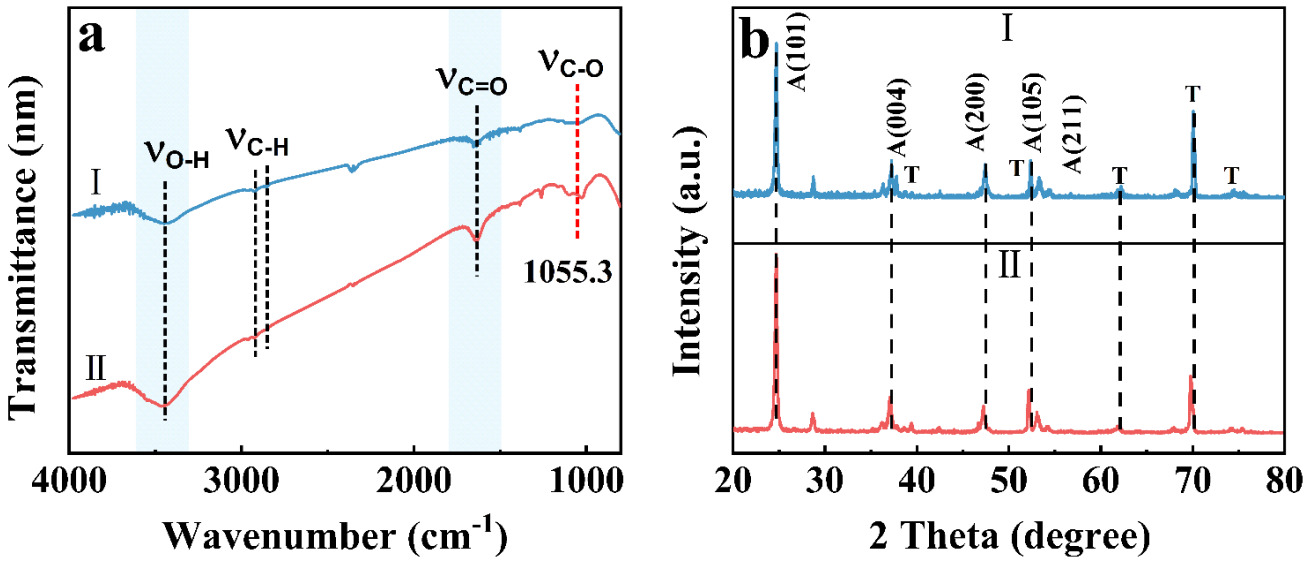

Fig. S20. (a) FTIR spectra and (b) XRD patterns of TNTAs@6P8A (I) before and (II) after cyclic reactions.

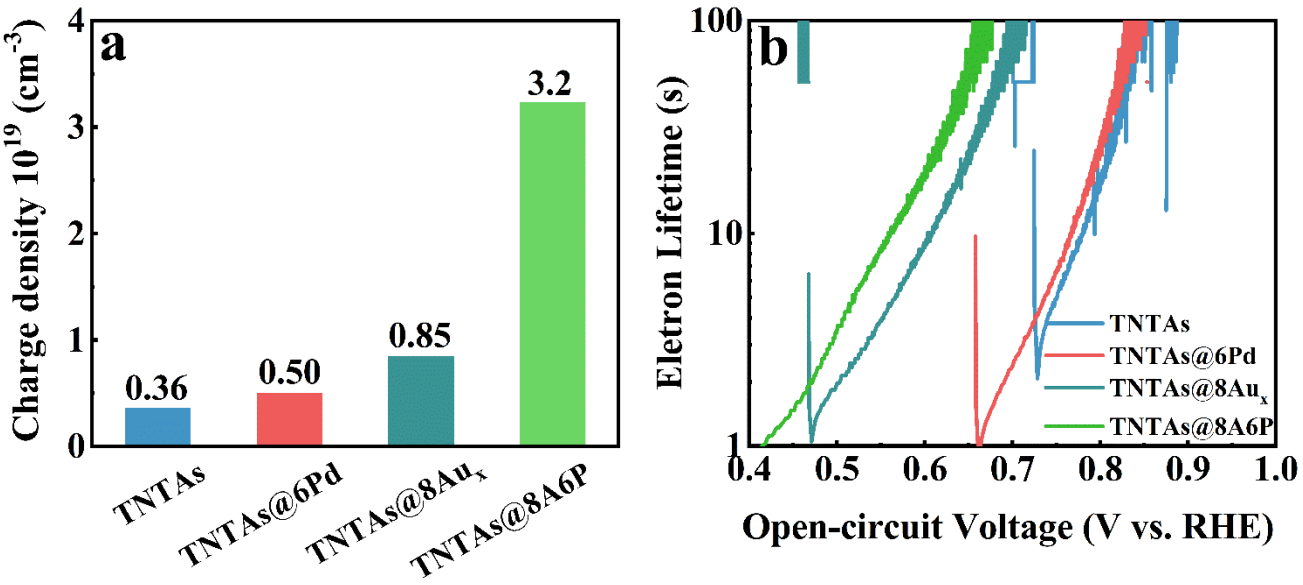

Fig. S21. (a) Charge carrier densities (N_D) and (b) electron lifetime of TNTAs, TNTAs@6Pd, TNTAs@8Au$_x$, and TNTAs@8A6P.

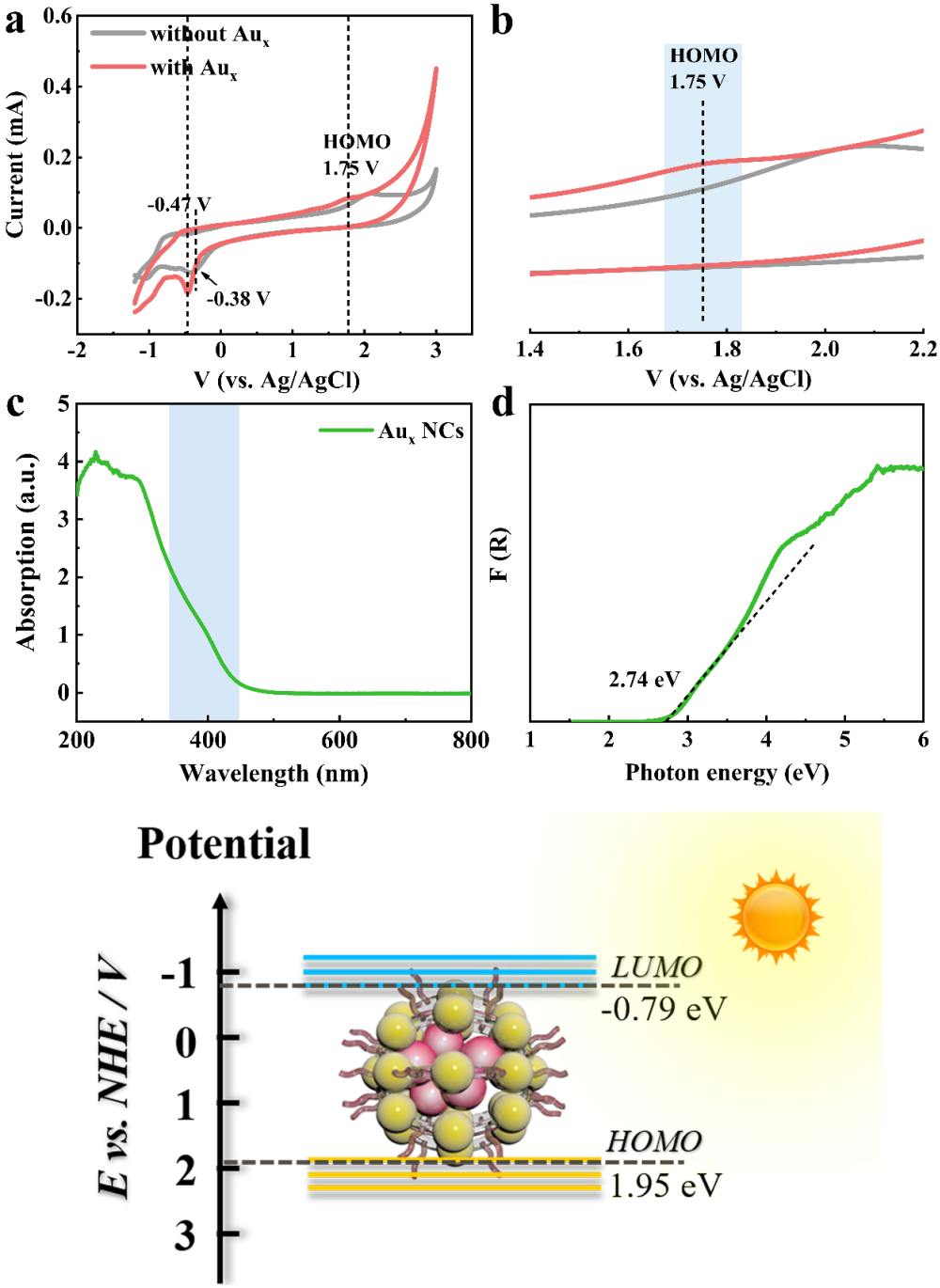

Fig. S22. (a) CV curves of Au_x@GSH NCs (electrolyte: degassed acetonitrile containing 0.1 mol L^{-1} TEAP); (b) magnified image; (c) UV-vis absorption spectra of Au_x@GSH NCs with (d) bandgap determination.

Note: CV curve of Au_x@GSH NCs shows an oxidation potential at 1.95 V (vs. NHE). Considering the bandgap of Au_x@GSH NCs (2.62 eV, **Fig. 1d**), LUMO level of Au_x@GSH NCs is determined to be -0.79 (vs. NHE). Thus, electrons photoexcited over Au_x@GSH NCs can flow from the LOMO level to the CB of TiO_2 (-0.53 V vs. NHE) in terms of favorable energy level alignment.

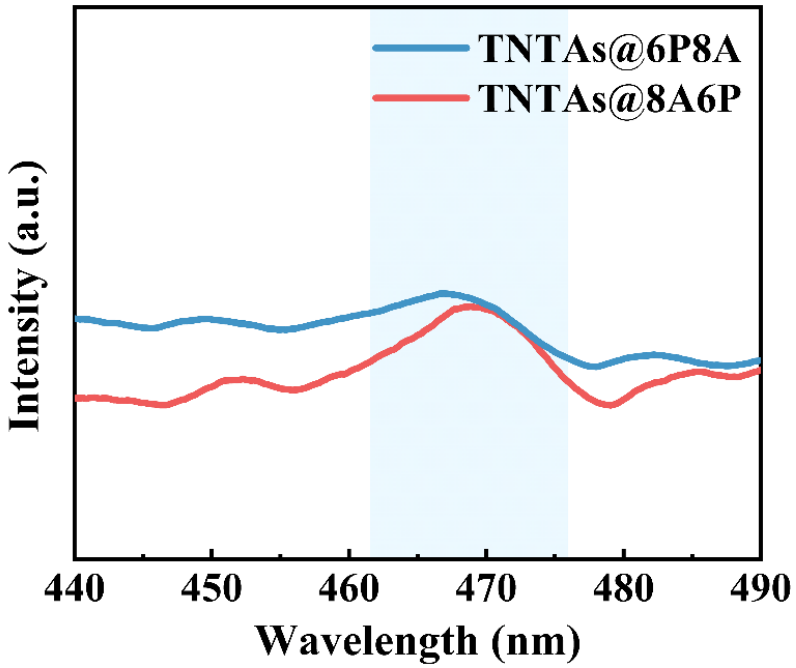

Fig. S23. PL spectra of TNTAs@8A6P and TNTAs@6P8A (λ_{ex}=450 nm).

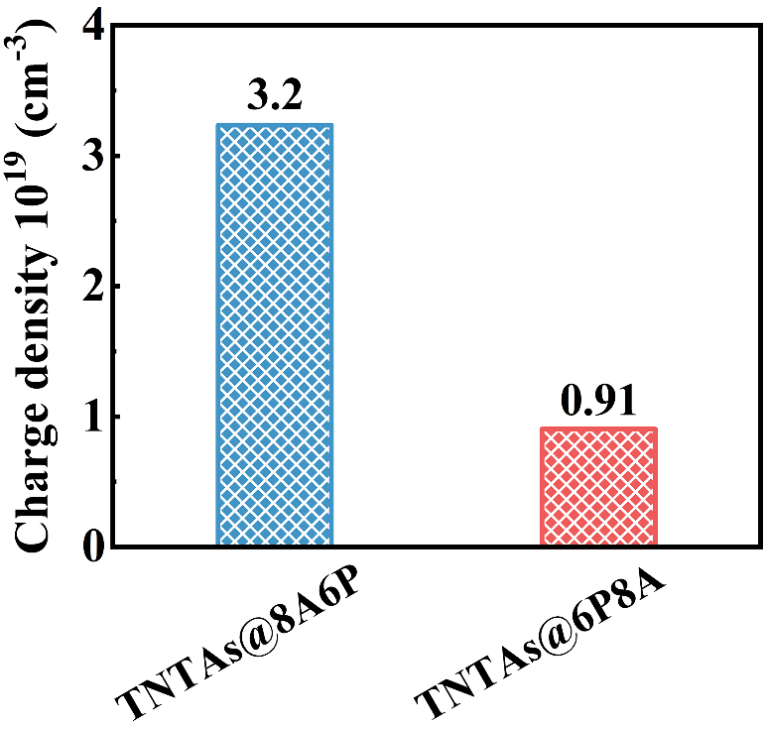

Fig. S24. Charge carrier densities (N_D) of TNTAs@8A6P and TNTAs@6P8A.

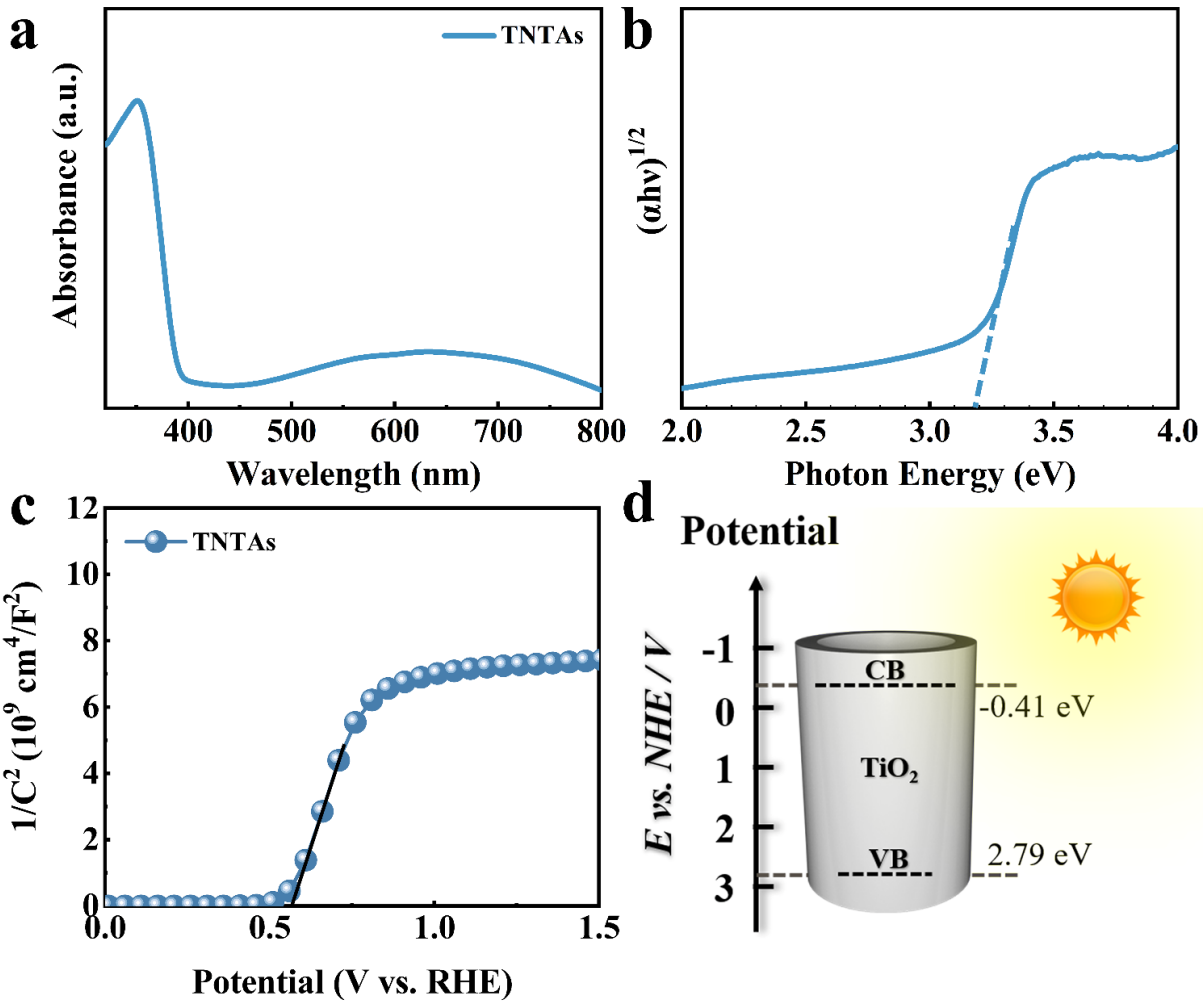

Fig. S25. (a) DRS results and (b) transformed plots based on the Kubelka-Munk function vs. the energy of light for TNTAs; (c) mott-Schottky plots; (d) energy level diagram of TiO_2.

Table S1. Peak position with corresponding functional groups.

Peak position (cm^{-1})	*Vibration mode*
3434.3	O-H stretching vibration [S10]
2923.6	C-H stretching vibration [S11]
2850.3	C-H stretching vibration
1628.5	C=O stretching vibration [S12]
1550.4	C=N stretching vibration [S11]
1388.5	Ti-O asymmetric vibrations [S10]

Table S2. Chemical bond species vs. B.E. for different samples.

Element	*TNTAs*	*TNTAs@6Pd*	*TNTAs@8A6P*	*Chemical Bond Species*
C 1s A	284.60	284.60	284.60	C-C/C-H
C 1s B	286.10	286.11	286.02	C-OH/C-O-C
C 1s C	288.16	288.05	287.86	Carboxylate (CO_3^{2-}) [S13-14]
Ti $2p_{3/2}$	458.29	458.30	458.31	Anatase (4+) [S15]
Ti $2p_{1/2}$	464.01	464.11	464.02	Anatase (4+)
O 1s A	529.55	529.56	529.46	Lattice Oxygen [S16]
O 1s B	531.19	531.41	531.09	Ti-OH
O 1s C	532.29	N.D.	532.16	-COOH
N 1s	N.D.	399.55	399.57	$-NH_2$/-NH- [S17]
	N.D.	N.D.	401.23	NH^{4+}
Pd $3d_{5/2}$	N.D.	335.88	335.28	Pd^0
Pd $3d_{3/2}$	N.D.	341.12	340.58	Pd^0
S $2p_{3/2}$	N.D.	N.D.	162.41	-SH
S $2p_{1/2}$	N.D.	N.D.	163.85	-SH
Au $4f_{7/2}$	N.D.	N.D.	83.38	Metallic Au^0
Au $4f_{5/2}$	N.D.	N.D.	87.03	Metallic Au^0
Au $4f_{7/2}$	N.D.	N.D.	84.36	Au^+
Au $4f_{5/2}$	N.D.	N.D.	88.04	Au^+

N.D.: Not Detected.

Table S3. A.Q.Y and S.T.H of TNTAs@8A6P, TNTAs@8Au_x, and TNTAs@6Pd at 365 nm.

Photocatalyst	*Light source*	*Activity (mmol·h^{-1})*	*A.Q.Y (%)*	*S.T.H (%)*
TNTAs@8A6P	365 nm	6.90	5.98	2.24
	400 nm	0.16	0.02	0.0094
	420 nm	0.048	0.0064	0.0028
	450 nm	0.062	0.0066	0.0034
	500 nm	0.063	0.0065	0.0034
	550 nm	0.065	0.0062	0.0033
	600 nm	0	0	0
TNTAs@6Pd	365 nm	6.4	5.6	2.07
TNTAs@8Au_x	365 nm	1.6	1.4	0.52
TNTAs	365 nm	0.23	0.20	0.074

Table S4. A.Q.Y and S.T.H of TNTAs@6Pd and TNTAs at 365 nm.

Photocatalyst	*Light source*	*Activity (mmol·h^{-1})*	*A.Q.Y (%)*	*S.T.H (%)*
TNTAs@6Pd	365 nm	6.4	5.6	2.07
	400 nm	0.053	0.0073	0.003
	420 nm	0	0	0
	450 nm	0	0	0
	500 nm	0	0	0
	550 nm	0	0	0
	600 nm	0	0	0
TNTAs	365 nm	0.23	0.20	0.074

Table S5. A.Q.Y and S.T.H of TNTAs@8Au_x and TNTAs at 365 nm.

Photocatalyst	*Light source*	*Activity (μmol·h^{-1})*	*A.Q.Y (%)*	*S.T.H (%)*
TNTAs@8Au_x	365 nm	1.6	1.4	0.52
	400 nm	0	0	0
	420 nm	0	0	0
	450 nm	0	0	0
	500 nm	0	0	0
	550 nm	0	0	0
	600 nm	0	0	0
TNTAs	365 nm	0.23	0.20	0.074

Table S6. A.Q.Y and S.T.H of TNTAs@6P8A, TNTAs@6Pd, TNTAs@8Au$_x$ at 365 nm.

Photocatalyst	*Light source*	*Activity (μmol·h^{-1})*	*A.Q.Y (%)*	*S.T.H (%)*
TNTAs@6P8A	365 nm	2.2	1.9	0.71
	400 nm	0	0	0
	420 nm	0	0	0
	450 nm	0	0	0
	500 nm	0	0	0
	550 nm	0	0	0
	600 nm	0	0	0
TNTAs@6Pd	365 nm	6.4	5.6	2.07
TNTAs@8Au$_x$	365 nm	1.6	1.4	0.52
TNTAs	365 nm	0.23	0.20	0.074

Table S7. Fitted EIS results of different photoanodes under simulated solar light irradiation based on the equivalent circuit.

Photoanode	R_s*/ohm*	R_{ct}*/ohm*	*CPE /(F·cm^{-2})*
TNTAs	49.88	3037	0.0004022
TNTAs@6Pd	36.28	2183	0.0004044
TNTAs@8Au$_x$	19.73	2114	0.0005146
TNTAs@8A6P	15.29	1484	0.000669
TNTAs@6P8A	21.46	1641	0.000426

Note: TNTAs@8A6P demonstrated the smallest R_{ct} value compared with other counterparts, indicative of its lowest interfacial charge transfer resistance.

Appendix

The self-designed automatic machine-based self-assembly apparatus utilized for super-efficient self-assembly of (a) TNTAs@8A6P and (b) TNTAs@6P8A heterostructures.

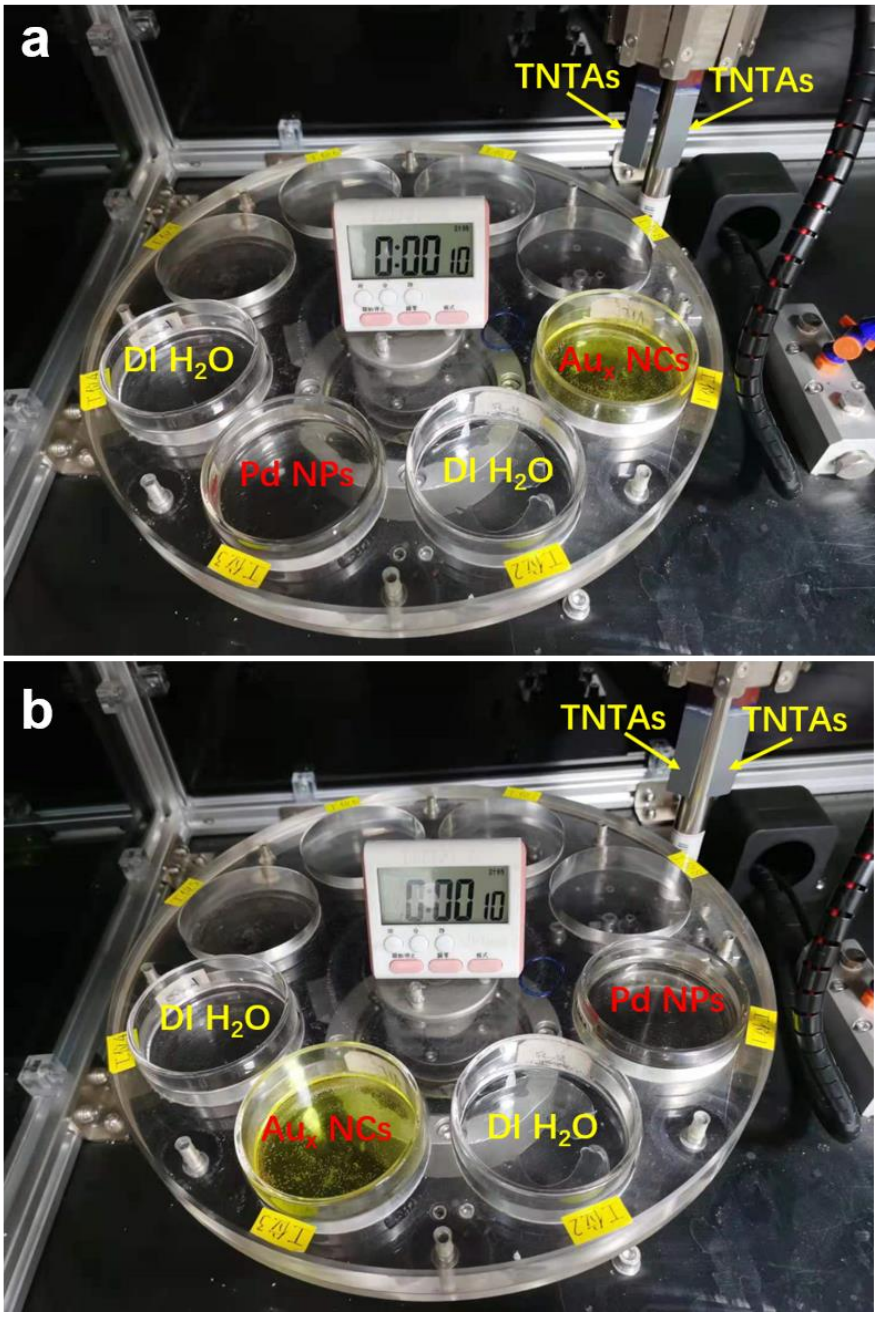

References

S[1] X.-C. Dai, M.-H. Huang, Y.-B. Li, T. Li, B.-B. Zhang, Y. He, G. Xiao, F.-X. Xiao, *J. Mater. Chem. A* 2019, **7**, 2741-2753.

S[2] N. Sakai, T. Tatsuma, *Adv. Mater.* 2010, **22**, 3185-3188.

S[3] D. I. Gittins, F. Caruso, *Angew. Chem. Int. Edit.* 2001, **40**, 3001-3004.

S[4] Y.-B. Li, T. Li, X.-C. Dai, M.-H. Huang, Y. He, G. Xiao, F.-X. Xiao, *J. Mater. Chem. A* 2019, **7**, 8938-8951.

S[5] M. Zhu, X. Cai, M. Fujitsuka, J. Zhang, T. Majima, *Angew. Chem. Int. Edit.* 2017, **56**, 2064-2068.

S[6] M.-H. Huang, X.-C. Dai, T. Li, Y.-B. Li, Y. He, G. Xiao, F.-X. Xiao, *J. Phys. Chem. C* 2019, **123**, 9721-9734.

S[7] T. Li, Y.-B. Li, X.-C. Dai, M.-H. Huang, Y. He, G. Xiao, F.-X. Xiao, *J. Phys. Chem. C* 2019, **123**, 4701-4714.

S[8] D. I. Gittins, F. Caruso, *Angew. Chem. Int. Edit.* 2001, **40**, 3001-3004.

S[9] F.-X. Xiao, Z. Zeng, B. Liu, *J. Am. Chem. Soc.* 2015, **137**, 10735-10744.

S[10] J. Li, S. Tang, L. Lu, H. C. Zeng, *J. Am. Chem. Soc.* 2007, **129**, 9401-9409.

S[11] B. B. Koleva, T. Kolev, R. W. Seidel, T. Tsanev, H. Mayer-Figge, M. Spiteller, W. S. Sheldrick, *Spectrochim. Acta A* 2008, **71**, 695-702.

S[12] F.-X. Xiao, S.-F. Hung, J. Miao, H.-Y. Wang, H. Yang, B. Liu, *Small* 2015, **11**, 554-567.

S[13] S. Biniak, G. Szymański, J. Siedlewski, A. Świątkowski, *Carbon* 1997, **35**, 1799-1810;

S[14] X. M. Wei, H. C. Zeng, *Chem. Mater.* 2003, **15**, 433-442.

S[15] F.-X. Xiao, *ACS Appl. Mater. Interfaces* 2012, **4**, 7055-7063.

S[16] F. Xiao, *J. Phys. Chem. C* 2012, **116**, 16487-16498.

S[17] F. Xiao, X. Luo, X. Fu, Y. Zheng, *J. Phys. Chem. B* 2013, **117**, 4893-4900.